UNIVERSIDADE FEDERAL DE PERNAMBUCO
DEPARTAMENTO DE FÍSICA – CCEN
PROGRAMA DE PÓS-GRADUAÇÃO EM FÍSICA

DISSERTAÇÃO DE MESTRADO

STUDY OF THE LONGITUDINAL SPIN SEEBECK EFFECT IN HYBRID STRUCTURES WITH YTTRIUM IRON GARNET AND VARIOUS METALLIC MATERIALS

Gabriel Andrés Fonseca Guerra

Recife
2014

UNIVERSIDADE FEDERAL DE PERNAMBUCO
DEPARTAMENTO DE FÍSICA – CCEN
PROGRAMA DE PÓS-GRADUAÇÃO EM FÍSICA

DISSERTAÇÃO DE MESTRADO

STUDY OF THE LONGITUDINAL SPIN SEEBECK EFFECT IN HYBRID STRUCTURES WITH YTTRIUM IRON GARNET AND VARIOUS METALLIC MATERIALS

por

Gabriel Andrés Fonseca Guerra

Dissertação apresentada ao Programa de Pós-Graduação em Física do Departamento de Física da Universidade Federal de Pernambuco como parte dos requisitos para obtenção do título de Mestre em Física.

Banca Examinadora:
Prof. Sergio Machado Rezende (Orientador - DF-UFPE)
Prof. Antonio Azevedo da Costa (DF-UFPE)
Prof. Alexandre Barbosa de Oliveira (ECT-UFRN)

Recife
2014

Catalogação na fonte
Bibliotecária Joana D'Arc L. Salvador, CRB 4-572

Fonseca Guerra, Gabriel Andrés.
Study of the longitudinal spin Seebeck effect in hybrid structures with yttrium iron garnet and various metallic materials / Gabriel Andrés Fonseca Guerra. – Recife: O Autor, 2014.
85 f.: fig., tab.

Orientador: Sergio Machado Rezende.
Dissertação (Mestrado) - Universidade Federal de Pernambuco. CCEN. Física, 2014.
Inclui referências e apêndice.

1. Matéria condensada. 2. Filmes finos. 3. Ferromagnetismo. 4. Platina. I. Rezende, Sergio Machado (orientador). II. Título.

530.41 (22. ed.) FQ 2014-29

Universidade Federal de Pernambuco
Departamento de Física – CCEN
Programa de Pós-Graduação em Física
Cidade Universitária - 50670-901 Recife PE Brasil
Fone (++ 55 81) 2126-7640/2126-8449
http://www.ufpe.br/ppgfisica e-mail: posgrad@df.ufpe.br

Parecer da Banca Examinadora de Defesa de Dissertação de Mestrado

Gabriel Andrés Fonseca Guerra

STUDY OF THE LONGITUDINAL SPIN SEEBECK EFFECT IN HYBRID STRUCTURES WITH YTTRIUM IRON GARNET AND VARIOUS METALLIC MATERIALS

A Banca Examinadora composta pelos Professores Sergio Machado Rezende (Presidente e Orientador), Antonio Azevedo da Costa, ambos do Departamento de Física da Universidade Federal de Pernambuco e Alexandre Barbosa de Oliveira, da Escola de Ciências e Tecnologia da Universidade Federal do Rio Grande do Norte, consideram o candidato:

(X) Aprovado ( ) Reprovado ( ) Em exigência

Secretaria do Programa de Pós-Graduação em Física do Departamento de Física do Centro de Ciências Exatas e da Natureza da Universidade Federal de Pernambuco, em dez de março de dois mil e catorze.

_____
Prof. Sergio Machado Rezende
Presidente e Orientador

_____
Prof. Antonio Azevedo da Costa

_____
Prof. Alexandre Barbosa de Oliveira

ACKNOWLEDGMENT

I want to express my sincere gratitude to the tutoring and guidance of my adviser Prof. Sergio Rezende from whom I learned not only physics but also invaluable professional values. I dedicate this work to my Parents Carlos Fonseca and Flor Guerra, to my wife Jaqueline and to my brothers Javier, Lore, Lili, Ingrid, Carito and Daniel who gave me the emotional support and all that I am in mind, heart and soul. Also I want to thank immensely to my wife who with her immense love and beauty give colors to this story in black and white and to God who give us strength to lift each new day.

In the technical aspects I would like to thank Prof. Sergio Rezende and Prof. Roberto Rodríguez by the construction of the magnon spin current theory for the LSSE, to Prof. Antonio Azevedo by invaluable discussions and to Ph.D. student Javier Lopez for the computation of the integrals and the relaxation rates. Also I am grateful to Prof. Fernando Machado, Prof. Alexandre Ricalde and Dr. Rafael Cunha for the help and orientation with the low temperature measurements and many details of the experiments with the spin Seebeck effect and microwave techniques. We acknowledge the support from the Conselho Nacional de Desenvolvimento Científico e Tecnológico, Coordenação de Aperfeicoamento de Pessoal de Nível Superior, Financiadora de Estudos e Projetos, and Fundacao de Amparo a Ciência e Tecnologia do Estado de Pernambuco.

we are free to spin, spin around our
decisions, dreams or projects, but only if
we spin around the true center, the
heart, the love, our spin will have the
correct orientation.

Gabirel Fonseca

ABSTRACT

In this master thesis we study experimentally the longitudinal spin Seebeck effect (LSSE) in bilayers made of a ferromagnetic insulator (FMI) and a metallic layer (M). We also present a theoretical model based on the spin current density $\vec{J}_s$ carried by a non-equilibrium magnon distribution, generated by a thermal gradient ∇T across the thickness of the FMI. When $\vec{J}_s$ reach the FMI/M interface it is pumped towards the M layer due to conservation of the angular momentum, so, the M layer is essential for the LSSE existence. Here the FMI consists of a Yttrium Iron Garnet (YIG) film, grown over a Gadolinium Gallium Garnet (GGG) substrate. Different metallic materials were used as the M layer i.e. Pt and Ta that have normal behavior and Py that is a ferromagnetic metal (FMM). The experimental procedure consists of systematic measurements of the electric voltage V_{ISHE}, produced by $\vec{J}_s$ through the Inverse Spin Hall Effect (ISHE) in the normal metal or (FMM) layer. In YIG/Pt measurements were done in the temperature range from 20 to 300 K. The experimental data are fitted to the proposed model for the LSSE and good agreement is obtained. The results shows that the Py and Ta can be used to detect the LSSE with the ISHE. The results of this master thesis have strong interest in the area of spin caloritronics helping to the development of the field and to raise possibilities of new spintronic devices.

Key-words: Spin Seebeck effect. Spin Hall effect. Magnon transport. Thin films. Pure spin current. Spintronics.

RESUMO

Nesta disertação é estudado experimentalmente o Efeito Seebeck de Spin Longitudinal (LSSE), em bicamadas formadas por um isolante ferromagnético (FMI) e um filme metalico (M). Também foi desenvolvido um modelo teórico baseado na densidade de corrente de spin $\vec{J}_s$ que existe quando uma distribuição de mágnons fora do equilíbrio é gerada por um gradiente térmico ∇T aplicado na secção transversal do FMI. Quando $\vec{J}_s$ chega na interface FMI/M é bombeada para a camada M satisfazendo a conservação do momentum angular, assim que a camada NM é essencial para ter um LSSE. Como camada FMI foi utilizada a granada de ítrio e ferro (YIG) crescida num substrato de (GGG). Diferentes materiais metalicos foram utilizados como camada M, sendo Pt e Ta paramagnéticos e o Py ferromagnetico. O procedimento experimental consiste na medição sistemática da voltagem elétrica V_{ISHE}, que é produzida por $\vec{J}_s$ por meio do efeito Hall de spin inverso (ISHE) que ocorre na camada M. As medidas em YIG/Pt foram feitas numa faixa ampla de temperatura de 20 a 300 K. Os dados experimentais são fitados com a teoria proposta para o LSSE encontrando-se boa concordância. Nossos resultados mostram que o Py e o Ta são bons candidatos para detecção do LSSE. Esta dissertação é de grande interesse na área da caloritrônica de spin, ajudando no desenvolvimento deste campo e na concepção de novos dispositivos tecnológicos baseados na spintrônica.

Palavras-chave: Efeito Seebeck de spin. Efeito Hall de spin. Transporte de magnons. Filmes finos. Corrente pura de spin. Spintrônica.

LIST OF FIGURES

CONTENTS

1. INTRODUCTION

From the birth of electronics with the invention of the vacuum diode by John Ambrose Fleming in 1904 and the vacuum triode by Lee De Forest in 1907, the operation of the devices was based in the energy and information transport by the charge of the electrons. This was done ignoring almost totally an intrinsic property of the electron, its spin, because it is randomly oriented in the conventional devices, hiding important phenomena. Electronics underwent a revolution with the discovery of the transistor in 1947. Since then the field has been evolving constantly. The development of the integrated circuits in semiconductor chips, doubling the number of transistors and resistors in each unit area every 12-18 months (tendency predicted by Gordon E. Moore, 19 April of 1965). In the last years this integration has reached the nanometric scale, but a conventional transistor can not be smaller than an atom, giving so, a natural limit to the electronic technology, as well as the difficulties that come from the Joule effect and thermodynamic bottleneck [11].

These facts bring the need of new ways of generating, storing and processing information. One possibility is to use a fundamental property predicted with the establishment of relativistic quantum mechanics by Paul A. M. Dirac, namely that the electron has an intrinsic angular momentum called spin, that is quantized and has an associated spin magnetic moment. This was confirmed by Stern and Gerlach in 1922 [12]. The new area of science and technology with information transport based in this property is called today spintronics or magneto-electronics.

The birth of spintronics is referred to the works carried out 0by Johnson and Silsbee in 1985 [13]. They showed experimentally, for the first time, the coupling between charges and spins in the interface of a ferromagnetic material (FM) with a paramagnetic metal (PM), achieving the injection and driving of spin in the latter.

All this, based in a method described conceptually by Aronov in 1976 [14], where a spin polarized current is emitted from the FM into the PM, taking advantage of the half-metallic nature of the Fermi surface in the band structure of the FM, so injecting in the metal a net magnetization that is proportional to the electric current I_e. Actually the Fermi surface has both types of bands, reducing the efficiency of the process. The magnetization current is given by:

$$I_m = \eta \mu_B I_e / e \tag{1.1}$$

where $\eta < 1$ is a phenomenological coefficient that describes the reduced efficiency of magnetization injection and μ_B, and I_e are respectively the Bohr magneton and the electric current. In fact in 1976 Meservey et al., [15], had realized an experiment in tunnel junctions made of a superconductor film, an oxide barrier and a ferromagnetic metal, with η between 0.1 and 0.5 This was much larger than the one found by Johnson and Silsbee with values of $\eta = 0.060 \pm 0.008$ and $\eta = 0.081 \pm 0.010$.

In 1986 Grünberg et al., (1986) observed for the first time the antiferromagnetic coupling between Fe layers separated by non-magnetic layers of Cr and taking as reference inter-layers of Au [16]. This sets the bases for the discovery of the giant magnetoresistance (GMR), that was realized simultaneously by the research groups of Grünberg (Binach et al., 1989) [17] and Fert (Baibich et al., 1988) [18]. This discovery let them to be awarded the Nobel prize in physics of 2007. Magnetoresistance (MR) is the change of the resistance in a conductor when submitted to an external magnetic field $\vec{H}$. In the case of the FM's this effect also depends on the direction of $\vec{H}$ relative to the direction of I_e, thus, receiving the name of anisotropic magnetoresistance (Thomson, 1856-1857) [19]. The effect is due to the spin-orbit coupling (s-o) of the electrons. The changes in the resistance are generally small but allow important technological advances, principally the development of the readout heads for magnetic disks as a field sensors, the most important was the permalloy $Fe_{20}Ni_{80}$ (Py). In the 1980's it was established that it was not possible to improve the magnetic sensors based on MR. Then the discovery of GMR by Grünberg and Fert made possible to overcome this limits reaching a decrease of almost 50% in the resistance with Fe/Cr multilayers. The introduction of GMR revolutionized the information storage techniques, the magnetic sensors and the research in magnetic thin films.

In the last 10 years the frontiers for the development of spintronic devices have been expanded, this because a set of new spin-related phenomena have been appeared promoted by distinct advancements in both, nanolithography and measurement techniques. The principal two new phenomena, that are directly related with this dissertation, are the electrical detection of the spin Hall effects, and the discovery of the spin Seebeck effect in metals, insulators and semiconductors. These effects allow the control, injection and detection of pure spin currents in conventional materials even in insulators. In this master dissertation we study experimentally and theoretically, the spin Seebeck effect in the longitudinal configuration in hybrid structures with yttrium iron garnet (YIG) and some metallic materials. Chapters 2-4 are devoted to the review the state of the art of the branch of the spintronic that deal with heat currents i.e. spin caloritronics. Due to the novelty of some phenomena, instead of presenting a rigorous and formal mathematical developments, we prefer to show the historical evolution that brought to us the problem of explaining the Spin Seebeck Effect. The concepts of pure spin current, spin pumping, spin transfer torque and spintronic trends and challenges are introduced in chapter 2. Chapter 3 is devoted to the Hall effects starting with the direct and anomalous and continuing with the spin Hall effects. The central subject of this work is the Spin Seebeck Effect that is studied in chapter 4, and in subsection 4.3.2 we introduce our theory for the Longitudinal Spin Seebeck Effect LSSE. In chapter 5 the experimental methods and procedures are described. The results so obtained are presented and analyzed in chapter 6. Finally the conclusions of this work close the dissertation.

2. SPIN TRANSPORT

This chapter is devoted to introduce the basic concepts of spin transport that will be fundamental for the development and understanding of this thesis. As we saw above the electrons have an intrinsic angular momentum called spin that is represented by the quantum operator $\vec{S}$ and that has an associated magnetic moment:

$$\vec{\mu} = g\mu_B\vec{S} = \gamma\hbar\vec{S}, \tag{2.1}$$

where g is the Landé factor, μ_B the Bohr magneton, γ the gyro-magnetic ratio and we have considered plus sign for $\vec{\mu}$, although some authors prefer the minus sign because the negative charge of the electron causes that the magnetic moment and angular momentum have opposite directions. Now, if a virtual surface is traversed by a net flux of angular momentum we can define a spin current in analogy with the charge current as:

$$\vec{I}_{Sv} = \frac{\partial\hbar\vec{S}}{\partial t} \tag{2.2}$$

and dividing by the area we have a spin current density:

$$\vec{J}_{Sv} = \frac{\hbar}{A}\frac{\partial\vec{S}}{\partial t}. \tag{2.3}$$

For understanding how J_{Sv} could be produced on a physical system, remember that in many body theory the Hamiltonian operator of a charged particle, under the action of electric and magnetic fields, is given by:

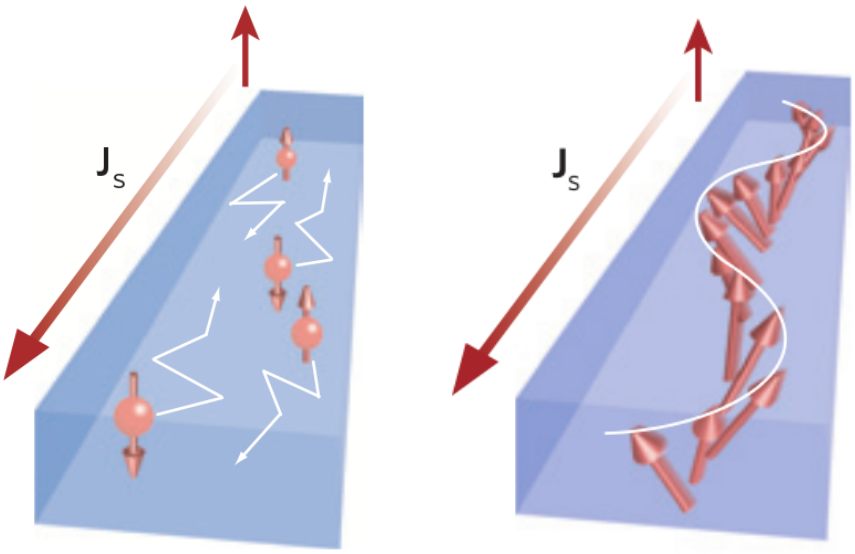

(a) conduction-electron spin current

(b) spin wave spin current

Figura 2.1: Representation of spin currents [figure 3 of ref [1]].

$$H = \sum_{i,\sigma} \frac{1}{2m} \left(P_i - \frac{e}{c} A_\sigma \right)^2 + \sum_{i \neq j} V_{i,j}, \tag{2.4}$$

where m, e and P_i are respectively the electronic mass, charge and momentum operator, c is the speed of light, A_σ is the spin-dependent vector potential operator with $\sigma = \uparrow, \downarrow$ the spin polarization, and $V_{i,j}$ electrostatic potential operator. For this Hamiltonian the velocity operators can be defined as [11]:

$$\nu_\sigma = \frac{1}{m} \sum_i \left(P_i - \frac{e}{c} A_\sigma \right) = -\frac{c}{e} \frac{\partial H}{\partial A_\sigma}. \tag{2.5}$$

With the eigenvalues $E(A_\uparrow, A_\downarrow)$ the electronic current is:

$$I_e = -e(\nu_\uparrow + \nu_\downarrow) = -e \left(\frac{\partial E}{\partial A_\uparrow} + \frac{\partial E}{\partial A_\downarrow} \right) \tag{2.6}$$

Let us consider two extreme cases, when $\nu_\uparrow = \nu_\downarrow$, all the electrons are moving

in the same direction regardless of the spin directions, thus $I_e = -2e\nu_\uparrow$ and $I_S = 0$. This is the common situation in conventional devices where the spins of electrons are oriented randomly and then the net flux of angular momentum is zero. A unique situation occur when $\nu_\uparrow = -\nu_\downarrow$, that is, electrons with opposite spins are moving in opposite directions. In this case $I_e = 0$, but $I_\sigma = \frac{\hbar}{2}(\nu_\uparrow - \nu_\downarrow) = \hbar\nu_\uparrow \neq 0$ the reason is that an up-spin moving to the right is equivalent to a down-spin moving to the left, giving rise to a pure spin current, a schematic representation of this effect is in Fig. 2.1 (a) [20, 21]. The latter effect appears in metals and semiconductors, although this is not the only situation that satisfies, $I_S \neq 0$. Another possibility is when the angular momentum is carried by collective spin precessions called spin waves, so that even in insulating materials can exist a spin transport. When some material presents a ferromagnetic nature (FM), even being insulator (without free electrons), its ions on the crystalline lattice have uncompensated spins, and in consequence a net magnetic moment, the volume average of this $\vec{\mu}$ is called magnetization:

$$\vec{M} = \frac{\sum_i \vec{\mu_i}}{\Delta V} = \gamma\hbar\frac{\sum_i \vec{S_i}}{\Delta V}, \tag{2.7}$$

where ΔV is the volume of the FM, then we can define a magnetization current density:

$$\vec{J_M} = \gamma\vec{J_S}. \tag{2.8}$$

A more useful equation for J_M can be found. The magnetization dynamics is governed by the Landau-Lifshitz equation, when we consider only the torque caused by an external magnetic field:

$$\frac{\partial\vec{M}}{\partial t} = \gamma\vec{M} \times \vec{H}_{eff}, \tag{2.9}$$

where $\vec{H}_{eff}$ is an effective molecular field. The relation 2.7 into 2.9, leads to:

$$\begin{aligned} \frac{\partial}{\partial t}\left(\gamma\hbar\frac{\sum_i \vec{S_i}}{\Delta V}\right) &= \gamma\left(\gamma\hbar\frac{\sum_i \vec{S}}{\Delta V}\right) \times \vec{H_{eff}} \\ \frac{\sum_i}{\Delta V}\frac{\partial}{\partial t}\hbar\vec{S_i} &= \frac{\sum_i}{\Delta V}\vec{\mu_i} \times \vec{H_{eff}} \end{aligned} \tag{2.10}$$

Here we can remember that a torque is defined as the temporal variation of angular momentum i.e. $\vec{\tau} = \frac{\partial \vec{L}}{\partial t}$. Then with 2.10, we have a spin torque equation:

$$\vec{\tau} = \frac{\partial \hbar \vec{S}}{\partial t} = \vec{\mu} \times \vec{H_{eff}}. \tag{2.11}$$

Using the divergence theorem we have the relation:

$$\int \frac{dV}{\gamma} \left(\frac{\partial \vec{M}}{\partial t} \cdot \hat{n} \right) = - \oint_S \vec{J}_S . d\vec{a} = - \int dV \nabla \cdot \vec{J}_S \tag{2.12}$$

and then:

$$\frac{\partial M}{\partial t} \cdot \hat{n} = -\gamma \nabla \cdot \vec{J}_S, \tag{2.13}$$

using 2.8, we obtain the continuity equation:

$$\frac{\partial M}{\partial t} \cdot \hat{n} = -\nabla \cdot \vec{J}_M. \tag{2.14}$$

This is a conservation equation that shows that the temporal variation of $\vec{M}$ lead to the generation of a magnetization or spin currents carrying information. Including the effects of J_M in L-L equation 2.9:

$$\frac{\partial \vec{M}}{\partial t} = \gamma \vec{M} \times \bar{H}_{eff} - \nabla \cdot \vec{J}_M. \tag{2.15}$$

On the other hand we can consider the exchange energy of the spin-spin interaction, that tray to keep any spin parallel to each other, L-L equation with exchange is written as:

$$\frac{\partial \vec{M}}{\partial t} = \gamma \vec{M} \times \bar{H}_{eff} - \gamma \frac{D}{M} \vec{M} \times \nabla^2 \vec{M}, \tag{2.16}$$

where D is the intraexchange stiffness parameter. Comparing 2.15 and 2.16 we note that:

$$\nabla \cdot \vec{J}_M = \gamma \frac{D}{M} \vec{M} \times \nabla^2 \vec{M} \tag{2.17}$$

and we can write:

$$\vec{J}_M = \gamma \frac{D}{M}(\vec{M} \times \nabla \vec{M}). \tag{2.18}$$

Additionally, the collective spin precessions or the magnetization dynamics on a FM, can be treated in terms of spin waves whose quantum is a pseudo particle called magnon and whose energy is determined by a wave vector $\vec{k}$ related to the frequency ω_k through a dispersion relation that in our case can be written as:

$$\omega_k = \gamma H + \gamma D k^2. \tag{2.19}$$

Conventionally the magnon system is approached with a second quantization formalism of Holstein Primakoff, then the number of magnons n_k in an statistical distribution is written in terms of the magnon creation and annihilation operators, $c_k^\dagger$ and c_k. Then, expressing $\vec{M}$ as:

$$\vec{M}(\vec{r}, t) = \hat{z}M + \hat{x}m_x(\vec{r}, t) + \hat{y}m_y(\vec{r}, t) \tag{2.20}$$

we make the transformation:

$$m^{\pm}(\vec{r}, t) = m_x(\vec{r}, t) \pm i m_y(\vec{r}, t). \tag{2.21}$$

Thus 2.18 take the form:

$$J^z_{Mv} = -\frac{i\gamma D}{2M}(m^- \nabla_v m^+ - m^+ \nabla_v m^-) \tag{2.22}$$

this equation allow the recognition of $m^\dagger$ as a wave function due to the similarity of 2.22 with the probability flux equation in quantum mechanics i.e. $\vec{j}(\vec{r}, t) = -\frac{i\hbar}{2m}[\Psi^*(\vec{r}, t)\nabla\Psi(\vec{r}, t) - \Psi(\vec{r}, t)\nabla\Psi^*(\vec{r}, t)]$. Thus we can make the transformation:

$$m^+ = \left(\frac{2\gamma\hbar M}{V}\right)^{\frac{1}{2}} \sum_k e^{ikr} c_k \qquad\qquad m^- = \left(\frac{2\gamma\hbar M}{V}\right)^{\frac{1}{2}} \sum_k e^{-ikr} c_k^\dagger, \tag{2.23}$$

and is easily shown that

$$\vec{J}_M^z = \frac{2\gamma D\gamma\hbar}{V}\sum c_k^\dagger c_k \vec{k} \tag{2.24}$$

or in terms of the group velocity of the magnons $\vec{v}_k = \partial\omega_k/\partial k = 2\gamma D\vec{k}$:

$$\vec{J}_M^z = \frac{\gamma\bar{h}}{V}\sum_k n_k\vec{v}_k \qquad or \qquad \vec{J}_s^z = \frac{\bar{h}}{V}\sum_k n_k\vec{v}_k; \tag{2.25}$$

from statistical mechanics point of view n_k is a distribution function and then 2.25 describe the spin transport on the FM, the spin current carried by spin waves is schematically represented in Fig. 2.1.

When we consider more than one material, and the spin currents reach the interface between adjacent materials, the transfer of spin will depend of the electric and magnetic nature of each material, In this master dissertation we will use the interface between a ferromagnetic insulator (YIG) and a normal (Pt, Ta) or ferromagnetic (Py) metals. If the spin current is generated on the FMI a spin pumping effect will occur at the interface, this phenomenon was described by Y. Tserkovnyak et al., in 2002 [22]. They use a NM/FM/NM junction and showed that when the magnetization in the FM starts precessing the Gilbert damping constant is enhanced when a spin current is pumped out of the ferromagnet [23]:

$$\vec{I}_s^{pump} = \frac{\hbar}{4\pi}\left(A_r\vec{m}\times\frac{d\vec{m}}{dt} - A_i\frac{d\vec{m}}{dt}\right). \tag{2.26}$$

Here $A \equiv A_r + iA_i$ is a complex value parameter i.e. the spin-pumping conductance, we can write $A = g^{\uparrow\downarrow} - t^{\uparrow\downarrow}$, that depends on the scattering matrix of the FM. The dimensionless dc conductance matrix is:

$$g^{\sigma\sigma'} \equiv \sum_{mn}[\delta_{nm} - r_{mn}^{\sigma}(r_{mn}^{\sigma'})*] \tag{2.27}$$

and

$$t^{\uparrow\downarrow} \equiv \sum_{mn} t_{mn}^{'\uparrow}(t_{mn}^{'\downarrow})* \tag{2.28}$$

where $r_{mn}^{\uparrow}$ ($r_{mn}^{\downarrow}$) is a reflection coefficient for spin-up (spin-down) on the NM, and $t_{mn}^{'\uparrow}$ and $t_{mn}^{'\downarrow}$ are the transmission coefficients for spin electrons across the FM film.

3. HALL EFFECTS

The development of the spintronics technology requires the existence of a bridge between the conventional electronics and those based on the spin, either for inclusion of spintronics sub-systems on the actual electronic devices, or for codification between both information systems. Also, as the research is conducted with electronic systems, we need a method for detect and inject spin currents from electric charge ones. This features are reached with the use of the Spin Hall Effect (SHE) and Inverse Spin Hall Effect (ISHE). In this chapter we will review the set of Hall effects and their importance to study the LSSE. We give a brief account of the historical developments that lead to the discovery of SHE and the ISHE. In this thesis the ISHE was fundamental to detect the pure spin current generated through the LSSE in the YIG/NM (NM= Pt, Py and Ta) structures.

3.1 Hall Effect and Anomalous Hall Effect

When Edwin H. Hall was reading the Maxwell's work on electricity and magnetism, he felt uncomfortable about the explanation of the effect of external magnetic fields on electric currents carried by conductors. So, in 1879 [24], he carried out experiments passing electric currents in a gold strip, mounted on a plate of glass between the poles of an electromagnet with the force lines orthogonal to the strip plane. He used a galvanometer to measure the existence of an electric potential generated transverse to the electric current, finding what today is known as conventional Hall Effect (HE), that has its origin on the Lorentz force of $\vec{H}$ over the conduction electrons. Subsequently he found this effect also in Ag, Sn, Pt, Fe and Ni, with the interesting result that the sign of the Hall voltage is inverted in some samples, in particular in the strong magnetic metals Fe and Ni. The exploration of

these phenomena gave rise to studies in Co and Ni showing that in ferromagnetic materials the HE had a strong contribution from the magnetization of the samples. This effect was called Anomalous Hall Effect (AHE) [25]. An empirical equation for the two Hall effects is:

$$E_h = R_0 H + R_1 M, \tag{3.1}$$

where E_h is the Hall electric field, H the applied magnetic field, M the magnetization and R_0 and R_1 are respectively the ordinary and anomalous Hall constants.

3.1.1 Intrinsic and Extrinsic Phenomena

The first quantum theoretical treatment of the origin of the AHE, was presented in 1954 by R. Karplus and J. M. Lutthinger who proposed that the root of the phenomenon arises from the spin-orbit coupling [26]. They used a hamiltonian with a periodic electric potential and included spin orbit interaction, considering interband matrix elements on the electronic band structure through time-dependent methods. They found a left-right asymmetry of the average velocity of the electron distribution, and use stationary states that was expressed as Bloch wave functions. Although these authors reached a good agreement with experiments, as shown by J. Smit [27], for have stationary current in presence of s-o interaction, lattice imperfections had to be introduced, and then the effect caused by the electric field is exactly canceled by the opposite action of the collisions against the imperfections. J. Smit showed in 1958 [27], that the AHE is caused by skew scattering.

In 1970 L. Berger postulated another mechanism for the AHE [28], taking into account that an electron involved in a s-o scattering could have a discontinuous and finite sideways displacement Δy, that through several interactions can become significant. The skew scattering and the side jump mechanisms are called extrinsic mechanisms because they occur during the s-o interactions. Recently it was proposed a universal intrinsic mechanism that exists even in a perfect lattice [29]. The central idea is that in the absence of scattering, it is possible to the s-o coupling to generate a spin-dependent anomalous velocity based only in the electronic band structure [29, 30, 31, 32, 33]. An important feature that allows the test of the emerging theories

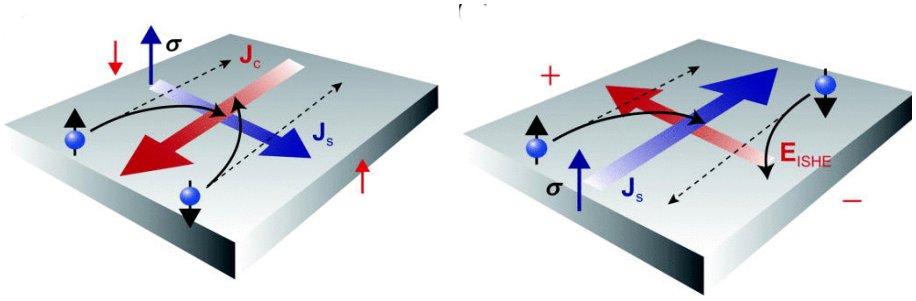

(a) SHE (b) ISHE

Figura 3.1: (a) A schematic illustration of the direct spin-Hall effect. Jc, Js, and σ denote a charge current, the spatial direction of a spin current, and the spin-polarization vector of the spin current, respectively. (b) A schematic illustration of the inverse spin-Hall effect. E_{ISHE}, J_s, and σ denote the electromotive force due to the inverse spin-Hall effect, the spatial direction of a spin current, and the spin-polarization vector of the spin current, respectively. [ref.[2]]

is the high dependence of the AHE with the temperature, generally associated with the resistance. In addition Y. Tian et al., found an empirical expression for the anomalous Hall conductivity [34]:

$$\sigma_{xy}^{AH} = -\left(\frac{\alpha}{\sigma_{xx0}} + \frac{\beta}{\sigma_{xx0}^2}\right)\sigma_{xx}^2 - b, \tag{3.2}$$

here σ_{xx} is the charge conductivity and σ_{xx0} is its contribution from residual impurities at low temperatures. Through this, they pointed out that the contribution from the three AHE mechanisms could be separated by the temperature scale, so the constants α, β and b corresponds respectively to the skew scattering, side jump and intrinsic contributions.

3.2 Direct and Inverse Spin Hall Effects (SHE-ISHE)

The theoretical understanding of the origin of the AHE through the skew scattering, allowed D'yakonov and Perel in 1971 [35] to predict that in a non-magnetic metals, some effect similar to the AHE can occur, However, as the spin moments are compensated, the charge carriers are deflected equally to both sides of the metal strip, then do not create a charge imbalance. The electrons at opposite sides have opposite spin polarities, which is interpreted as spin accumulation at the extremes of the strip. Thus, we can generate a pure spin current through a pure charge current. Formally we have the drift diffusion equations for charge and spin currents:

$$\frac{\vec{j}^c}{e} = \mu n \vec{E} + D\vec{\nabla} n, \tag{3.3}$$

$$\frac{j^s_{ij}}{\hbar} = -\mu n E_i P_j + D\frac{\partial P_j}{\partial x_j}, \tag{3.4}$$

where μ is the electron mobility, $\vec{E}$ is the electric field, n is the electron density, D is the electron diffusion constant and j^s_{ij} is the spin current tensor, with the j component of the spin polarization density $\vec{P}$ flowing in the direction i. For materials with inversion symmetry we can define spin and charge currents from 3.3 and 3.4 to be:

$$\frac{j^c}{e} = \mu n \vec{E} + D\vec{\nabla} n + \Theta_{SH}\mu(\vec{E} \times \vec{P}) + \Theta_{SH} D(\vec{\nabla} \times \vec{P}) \tag{3.5}$$

$$\frac{j^s_{ij}}{\hbar} = -\mu n E_i P_j + D\frac{\partial P_j}{\partial x_j} - \epsilon_{ijk}\left(\Theta_{SH}\mu n E_k + \Theta_{SH} D\frac{\partial n}{\partial x_k}\right). \tag{3.6}$$

These equations are coupled in a way that in 3.5, the third term describes the AHE in the presence of a net spin polarization $\vec{P}$ and the fourth term give the inverse spin hall effect (ISHE), i.e., the generation of a charge current through a spin current. Here Θ_{SH} is the spin Hall angle defined as the ratio of the spin and charge conductivities:

$$\Theta_{SH} = \frac{\sigma^s_{xy}}{\sigma^c_{xx}} \frac{e}{\hbar}, \tag{3.7}$$

where by definition $\sigma^c_{xx} = ne\mu$ and similarly $\sigma^s_{xy} = n\hbar\mu\Theta_{SH}$. The most common equation used for experiments with ISHE is [36]:

$$\vec{J_c} = \Theta_{SH} \frac{2e}{\hbar} \vec{J_s} \times \sigma. \tag{3.8}$$

For obtain the equations 3.5 and 3.6 is used the continuity equation for the spin density $\vec{S}$:

$$\frac{\partial S_\beta}{\partial t} + \frac{\partial q_{\alpha,\beta}}{\partial x_\alpha} + \frac{S_\beta}{\tau_s} = 0, \tag{3.9}$$

where τ_s is the spin relaxation time and $q_{\alpha,\beta}$ is the spin flux density tensor, indicating the flux of the β-component of the spin in the α direction:

$$q_{\alpha,\beta} = -b_s E_\alpha S_\beta - d_s \frac{\partial S_\beta}{\partial x_\alpha} + \beta_s n \epsilon_{\alpha\beta\gamma} E_\gamma, \tag{3.10}$$

or

$$\vec{q} = -bn\vec{E} - \delta\nabla \times \vec{S} - \beta \left[\vec{E} \times \vec{S}\right], \tag{3.11}$$

with $\vec{E}$ the electric field, n the electronic density and $\epsilon_{\alpha\beta\gamma}$ is the Levi-Civita tensor. In this equations the constant b_s is the spin mobility and its term describes the drift of spin caused by $\vec{E}$, d_s is the spin diffusion and β_s is the spin-electric coefficient, its term take account of the transverse spin flux caused by the s-o interaction or AHE.

After this theoretical achievement N.S. Averkiev and M.I. D'yakonov proposed in 1983 [37] an experimental approach to detect the ISHE, following this proposal Bakun et al., published, in 1984, the experimental achievement [38]. Thus, in the n-type direct-band semiconductor $Ga_{0,73}Al_{0,27}As$, the orientation of electron-spins, through the interband absorption of circularly polarized light from an helium-neon laser, generate a gradient in the spin density, giving rise to a diffusion spin flux away from the surface. This spin current is asymmetrically scattered by charged impurity centers originating a electric current. This was the first observation of the ISHE effect. The names of Spin Hall Effect (SHE) and Inverse Spin Hall Effect

(ISHE) was coined by J. E. Hirsch who without knowledge of the D'yakonov and Perel works, made a theoretical deduction of the effects in 1999 [39].

In 2004 Y. K. Kato et al., [40], use the Kerr rotation microscopy to observe the extrinsic SHE in series of semiconductors samples fabricated from $n - GaAs$ and $n - In_{0.07}Ga_{0.93}As$ films grown on (001) semi-insulating GaAs substrate by molecular beam epitaxy. additionally was found that strain modifies spin accumulation at zero magnetic field and the weak dependence on crystal orientation for the strained samples, reveal that is the extrinsic spin Hall effect the principal mechanism. The next year Azevedo et al., [41] made the first electrical detection of the ISHE in metals using ferromagnetic resonance (FMR) in FM/NM/FM trilayers of $Py/NM/Fe_{50}Co_{50}$ where $NM = Cu,\ Pd,\ Ta$ and W. They found that the ISHE increases with the atomic number of the element used for the NM layer. In the following year Saitoh et al., showed similar measurements in FM/NM bilayers and interpreted this observations in terms of spin pumping and spin Hall effects [36, 42, 43, 44]. In the same year J. Wunderlich et al., [45], observed the SHE in a two-dimensional s-o coupled semiconductor which is part of a p-n junction light emitting diode with a co-planar geometry. Using quantum transport calculations it was suggested that the effect is of intrinsic nature. In 2006 Valenzuela and Tinkham realized direct electronic measurements of the SHE with a tunnel barrier to inject a spin-polarized current in Al.

One of the initial limitations of these effects is that the efficiency of interconversion was in the best cases a few percent [46] although recently studies in tantalum and tungsten apparently show a high improvement of efficiency [47, 48]. An interesting advance was published by B. F. Miao, namely, the existence of ISHE in a FM metal i.e. Permalloy in the system YIG/Py with the Py presenting a large spin Hall Angle [42]. Thus, one of the great advantages of the SHE is the possibility of injection of spin currents and manipulation of the magnetization, even in insulator materials as these can not be made with electrical injection [49].thus the spin Hall effects allow the active use of the non-magnetic metals in spintronics devices. A very good review in this topic was published by Axel Hoffmann in ref. [50].

4. SPIN CALORITRONICS

The endeavor to control the heat transport in nano- and micro-structures are summarized in the term *caloritronics*, that comes from "calori- + electronics". When this thermoelectric transport exists in systems with non-equilibrium spin populations, one has what is called *Spin Caloritronics*. This research field was formally stated and reviewed in references [1, 51, 52]. Due to the experimental difficulties for the control of heat flows, this thermoelectric spintronics took time to gain strength, although the technological implication in information processes and storage systems is huge and have a environmentally friendly character.

In thermoelectrics is stated that in a diffusive metal the electrical and thermal forces are related through [53]:

$$\begin{bmatrix} \vec{E} \\ \vec{Q} \end{bmatrix} = \begin{bmatrix} 1/\sigma_e & S \\ \Pi & \kappa \end{bmatrix} \begin{bmatrix} J_c \\ -\nabla_r T \end{bmatrix}, \tag{4.1}$$

where $\vec{E}$ is the electric field, $\vec{Q}$ is the heat current, σ_e is the electric conductivity, T the temperature and κ the heat conductivity. The coefficients Π and S are respectively the Peltier and Seebeck coefficients that quantified the transformation of $\vec{E}$ into $\vec{Q}$ and vice versa. In 1931 Lars Onsager published his reciprocal relations for irreversible processes, in essence he demonstrated that the matrix of phenomenological coefficients $L_{\alpha\beta}$ for transport phenomena is a positive semi-definite matrix and is also symmetric. This allow to demonstrate the second Thomson relation, i.e. $\Pi = ST$, being the Seebeck and Peltier effects reciprocal. In a FM material the thermoelectric properties have to consider conductivities that depend of the spin, so the charge conductance is:

$$\sigma = \sigma^{(\uparrow)} + \sigma^{(\downarrow)} \tag{4.2}$$

and the Seebeck coefficient become:

$$S = \frac{\sigma^{(\uparrow)} S^{(\uparrow)} + \sigma^{\downarrow} S^{(\downarrow)}}{\sigma^{(\uparrow)} + \sigma^{\downarrow}}, \tag{4.3}$$

then the Eq.4.1 can be extended to include spin transport [54]:

$$\begin{bmatrix} \vec{J}_c \\ \vec{J}_s \\ \vec{J}_Q \end{bmatrix} = \sigma \begin{bmatrix} 1 & P & S \\ P & 1 & P'S \\ ST & P'ST & \kappa/\sigma \end{bmatrix} \begin{bmatrix} \Delta\mu_c/e \\ \Delta\mu_s/e \\ -\Delta T \end{bmatrix}, \tag{4.4}$$

where μ_c and μ_s are respectively, the charge and spin chemical potentials, P and P' are the spin polarization of the conductivity and its energy derivative:

$$\begin{aligned} P &= \frac{\sigma^{(\uparrow)} - \sigma^{(\downarrow)}}{\sigma} \mid_{E_F}, \\ P' &= \frac{\partial(P\sigma)}{\partial E} \mid_{E_F} . \end{aligned} \tag{4.5}$$

The symmetry of the spin-dependent thermoelectric matrix 4.4 is in accordance with the Onsager's reciprocity relations, and so the interconvertion between charge, spin and heat currents is allowed, actually this is the challenge of the Spin caloritronics.

The origin of spin caloritronics goes back onto the year of 1987 with the Johnson and Silsbee works of non-equilibrium thermodynamics of spin, charge and heat in metallic hetero-structures [54]. Thereafter, in 1991 Junji Sakurai et al., measured effects of the magnetic field, $\vec{H}$, on the thermoelectric power (TEP) of GMR-metallic multilayers, finding large magneto-thermopowers MTP [55]. Jing Shi et al., in 1996 searching the underlying mechanism behind the GMR, presented measurements of its dependence with $\vec{H}$, and the correlation with the thermal conductivity and TEP on multilayers and granular systems [56]. They also proposed a model in which the resistivity ρ and TEP are dominated by the scattering of the non-magnetic s bands

into the magnetic d bands. In 2003 M. Johnson presented a thermodynamic study of spin injection and Charge–Spin Coupling at a FM/NM interface [57]. Two years later Akio Fukushima et al., studied the cooling power, through the Peltier effect, in metallic GMR trilayers with the current parallel to the plane [58].

Oleksandr Tsyplyatyev et al., in 2006 showed that thermally excited spin currents appear in metals with embedded ferromagnetic nano-clusters, with the spin currents observed via a giant MTP [59]. This same year, Laurent Gravier et al., studied the spin-dependent heat and charge transport in Co/Cu multilayers carrying a dc electric current through the sample, and measuring the ac voltage resulting from a thermal small oscillation [60]. This work showed a magnetic response 50% larger than GMR, introducing a new experiment, that they called magneto-thermogalvanic voltage (MTGV). They explained the results reducing the number of free parameters with the Onsager reciprocal symmetry relations and using a three-current model i.e. spin up, down and entropy currents.

In 2007 Moosa Hatami et al., predicted that in metallic spin valves, a spin-polarized thermoelectric heat current could produce a magnetization reversal from spin transfer torque (STT) [61]. In 2008 K. Uchida et al., discovered the Spin Seebeck effect (SSE) also called by some authors thermo spin effect. The discovery gave rise to a large number of works in this subject, but as the central phenomena involved in this master thesis, we procrastinate the next sections for a more complete study of the SSE.

On the other hand Moosa Hatami et al., studied theoretically in 2009 the Seebeck and Peltier thermoelectric effects in magnetic multilayer nanostructures [62]. For this, they used classical approaches for thermoelectrical transport including spin relaxations, predicting the magneto-Peltier effect in spin valves. In the same year Alexey A. Kovalev and Yaroslav Tserkovnyak suggested that magnetic texture dynamics could generate a cooling effect [63]. In 2010, with the aim of enlarge the efforts to search the missing answers in spin caloritronics and generate realistic applications to devices, a complete volume of the *Solid State Communications* journal was devoted to Spin caloritronics. Our references [52], [64, 65, 66, 67, 68, 51, 69, 70, 71, 72, 73, 74, 75, 76, 77, 78], belong to this volume and some are summarized below, the others are included in the SSE section (3.3.1).

One of the important topics is the adaptation of the experimental approaches to the novelty of the recent discoveries. With this motivation, R. Huber et al., introduced techniques to explore the coupling between different degrees of freedom in spin caloritronics and magneto-mechanics, with all-electrical spectroscopy, allowing the study of the phonon-magnon interaction [64]. Another progress was made by B. L. Zink, who developed a thermal micro-machined platform capable of measuring both, thermal conductivity, Seebeck coefficient, and electrical conductivity [65].

Another experimental achievements was conducted by T. Seki et al., who report experimental evidence for thermal spin-related Hall effects in multi-terminal devices consisting of a FePt/Au hetero-structures [66]. B. Balke measured the Seebeck coefficient, from low to room temperatures, for Co_2 based Heusler compounds and were discussed as potential materials for spin voltage generation [79]. In 2010 Heming Yu et al., reached the generalization of heat and spin transport to non-collinear configurations. They showed the experimental evidence in Co/Cu/Co spin valves and suggested a technological alternative to the reverse of the magnetization using external magnetic fields in high density and low power magnetic memories [80].

On the theoretical side, through the Rashba s-o interaction was predicted an intrinsic thermo-spin Hall effect, or spin Nernst Effect, i.e., a transverse spin current generated by some ∇T and a heat current in a disorder-free two-dimensional electron gas (2DEG). The problem was studied analytically and numerically in absence of a external $\vec{H}$. The interplay between the spin Nernst effect and the Seebeck effect was also investigated in ref's [67, 68]. To describe the spin-transfer effect, Wegrowe et al., extended the Johnson-Silsbee approach to non-collinear magnetic structures, and give a study of the irreversible process present in spintronic devices, clarifying the nature of the power dissipated in metallic ferromagnets when contacted to a electric generator [69]. The analysis is of statistical mechanics nature, and present a generalization of the Landau -Lifshitz equation to spin-accumulation.

Kjetil M. D. Hals et al., [70] used scattering theory in the ferromagnetic semiconductor (Ga, Mn)As for study the domain wall motion (DWM) induced by a ΔT and the reciprocal effect of heat currents pumped by a DWM. Here a $\nabla T = 100-1000\, K/\mu m$ generates a $V_{DM} = 10m/s$ and a $V_{DM} = 10m/s$ pumps $\approx 0.2w/m^2$, although they found that this DW system is not useful for cooling, A.A. Kovalev

and Y. Tserkovnyak in 2009 [63], propose theoretically the construction of magnetocaloritronic nanomachines for cooling and power generation, suggesting that FM insulators could give better efficiencies than the FM metals. The thermal fluctuations of this DW in terms of Brownian motion generate a spin motive forces that could be characterized through the noise spectrum in the induced current. Experimental results in this topic were obtained by magneto-optical Kerr-microscopy in 2010 [71], generating a field-induced DWM and pinning in Py microwires under the influence of ∇T. W. Jiang et al., in 2013, used the same technique to observe the phenomenon with spatio-temporal resolution in samples of YIG/Pt finding that the DW moves towards the Hot regime and that exist a threshold for the ∇T that causes DWM [81]. Z. Yuan et al., used the Landauer-Büttiker formalism to do a first principles determination of the STT caused by this thermal induced DWM [72].

It was realized theoretically that the spin caloritronic transport is affected by inelastic scattering. Thus electron–electron interaction induce spin thermalisation in quasi-low-dimensional spin valves [73]. Yonatan Dubi and Massimiliano Di Ventra studied SSE in a nanojunction composed of two ferromagnetic leads attaching a quantum dot [82]. The nanojunction can be tuned to supply pure spin currents. Founding the Seebeck coefficient, S_s, and the figure of merit. They suggested that the spin and charge Seebeck coefficients are of the same order of magnitude, while the measures of ref [83] measure a S_s with four orders of magnitude lower than S_c. On the other hand, M. Hatami et al., showed that use of a simple semi-classical theory of spin diffusion, based on the Boltzmann equation, do not explain the SSE in a ferromagnetic metal [74], lacking a full theory for SSE.

Chih-Piao Chuu et al., [75] provide a semi-classical approach, from the Dirac electron model, for understand dynamics and transport phenomena related to spin in solids, as well as the fundamental nature of the electron spin, the so obtained Berry curvature introduce anomalous velocities and so the spin Nernst Effect and the SHE's. Other examples of useful first principle calculations and computational methods for spin caloritronics are found in ref's [72, 76, 84]. Finally, an interesting feature of the spin caloritronics, is that could be extended beyond the solid state structures, being predicted in cold atomic gases [85].

4.1 Spin Seebeck Effect in Ferromagnetic Metals

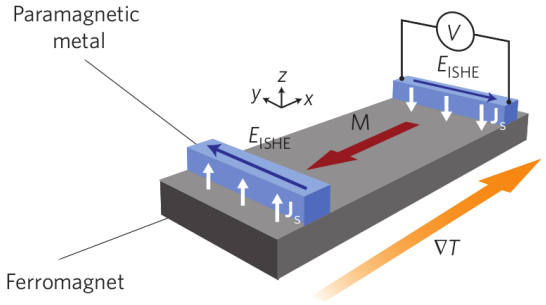

Figura 4.1: Transverse Spin Seebeck Effect configuration [Fig. 3 of ref [37]].

In 1821 Thomas Johann Seebeck discovered the thermoelectric effect that today has his name (SE), and that consists in the generation of an electric voltage when two dissimilar metals are joined in one extreme and a gradient of temperature is applied between the ends of the junction [86, 87, 88, 89]. At that time Seebeck explained his observation as a thermomagnetic effect without considering an electric current, but today the thermoelectrical nature of the experiment is well established [90]. The SE is quantified by a Seebeck coefficient S, that is the ratio of the electric voltage to the temperature difference that generate this voltage, $S = \frac{\Delta V}{\Delta T}$.

In 2008 K. Uchida et al., published the first observation of the spin-dependent thermoelectrical phenomena that they called spin Seebeck effect (SSE), because of the similarity with the classical thermoelectrical SE [83]. This time the temperature gradient produce a spin voltage on the extremes of the metal strip, through spin pumping, this system can inject a pure spin current J_S^P in an adjacent material. The system used by K. Uchida et al., was a metallic ferromagnetic film of Py with a wire of Pt sputtered on one end. The sample was submitted to an in-plane static magnetic field parallel or anti-parallel to ∇T which is perpendicular to J_S^P, in this geometry, called transverse configuration (TSSE), see Fig.4.1, the Nernst effect is avoided. The Pt wire works as a sensor through the ISHE, since a spin current is injected from the Py and converted in a transverse electric current read by a conventional nonovoltmeter. Initially they use a phenomenological explanation using the concept of electrochemical potential for spin-up and spin-down electrons, $\mu \uparrow$

and $\mu\downarrow$, and consider the fact that different scattering rates could generate different spin-dependent driving powers. They state that the spin voltage at the hot end of the sample that have a temperature difference ΔT at its extremes is given by$V_s = (\mu\uparrow - \mu\downarrow) = eS_s\Delta T/2$, where S_s is the spin Seebeck coefficient. A relevant characteristic is that J_S inside the magnet is produced over long distances and without electric currents.

4.1.1 Phenomenological Analysis of the Spin Seebeck Effect In Metallic Ferromagnets

The next year they proposed a thermodynamic phenomenological analysis for SSE in metallic magnets ref [91]. Two features have to be reproduced by the model. First, The spin voltage have (V_s) opposite signs at the ends of the FM and second, the value of V_s varies linearly along the direction of ΔT. The explanation is based in the concepts of electrochemical potential for conduction electrons μ_σ, where σ is the polarization of the spins, thus we have:

$$V_s = \mu_\uparrow - \mu_\downarrow, \tag{4.6}$$

cause the spin movements characterized by the spin-diffusion length λ. The equation for the spin diffusion was found by T. Valet and A. Fert [92]:

$$\nabla^2(\mu_\uparrow - \mu\downarrow) = \frac{1}{\lambda^2}(\mu_\uparrow - \mu\downarrow), \tag{4.7}$$

but this equation had to be extended for account for the SSE observations. We need a equation that take in account the non-steady states created by ∇T. Equation 4.7 was derived from:

$$\nabla\mu_\sigma = \frac{1}{N_\sigma}\nabla n_\sigma - e\nabla\phi, \tag{4.8}$$

where N_σ, n and ϕ are respectively the spin- dependent density of state, carrier density, and the electrostatic potential. In 4.8 was considered that μ_σ is non dependent

of the entropy S. And for explain the SSE K.Uchida et al., include the contribution of S expanding the gradient of μ_σ in the form:

$$\nabla\mu_\sigma = \left(\frac{\partial\mu_\sigma^c}{\partial T}\right)\nabla T + \left(\frac{\partial\mu_\sigma^c}{\partial n_\sigma}\right)\nabla n_\sigma - e\nabla\phi \tag{4.9}$$

$$\equiv \left(\frac{\partial\mu_\sigma^c}{\partial T}\right)\nabla T + \nabla\bar{\mu_\sigma}, \tag{4.10}$$

the three terms of this equation represent the entropy, carrier-density and electric field contributions, in our case ∇T is uniform so 4.10 become:

$$\mu_\sigma = \left(\frac{\partial\mu_\sigma^c}{\partial T}\right)_{n_\sigma}(\nabla T)x + \bar{\mu}_\sigma + C, \tag{4.11}$$

where C is an integral constant. This expression allow to expand the Valet-Fert equation to:

$$\nabla^2(\mu_\uparrow - \mu_\downarrow) = \frac{1}{\lambda^2}(\mu_\uparrow - \downarrow) - \frac{e}{\lambda^2}S_s(\nabla T)x, \tag{4.12}$$

where S_s is the spin Seebeck coefficient:

$$S_s \equiv \left(\frac{1}{e}\right)\left[\left(\frac{\partial\mu_\uparrow^c}{\partial T}\right)_{n_\uparrow} - \left(\frac{\partial\mu_\downarrow^c}{\partial T}\right)_{n_\downarrow}\right], \tag{4.13}$$

and determine the efficiency of the spin voltage induced thermally. The solution of 4.12 have the form:

$$\mu_\uparrow - \mu_\downarrow = eS_s(\nabla T)x + A\,sinh(x/\lambda), \tag{4.14}$$

where $A = -e\lambda[S_s - (S_\uparrow - S_\downarrow)]\nabla T/cosh(L/2\lambda)$, the used boundary conditions were $\vec{j}_s(x = \pm L/2) = 0$, being L the length of the FM. In this way is found:

$$\vec{j}_s = \frac{\sigma_F}{2}(1 - p_c^2)[S_s - (S_\uparrow - S_\downarrow)].\left[1 - \frac{cosh(x/\lambda)}{cosh(L/2\lambda)}\right]\nabla T \tag{4.15}$$

where $\sigma_F = \sigma_\uparrow + \sigma_\downarrow$ and $p_c \equiv (\sigma_\uparrow - \sigma_\downarrow)/(\sigma_\uparrow + \sigma_\downarrow)$. If the condition $L >> \lambda$ is satisfied, as conventionally, the equations 4.15 and 4.14 transformed into:

$$\mu_\uparrow - \mu_\downarrow = eS_s(\nabla T)x \tag{4.16}$$

$$\vec{j}_s = \frac{\sigma_F}{2}(1-p_c^2)[S_s - (S_\uparrow - S_\downarrow)]\nabla T. \tag{4.17}$$

Then the expansion of Valet-Fert equation to include the entropy effects lead to the equations. 4.17 that describe well the experimental features of the SSE.

4.2 Spin Seebeck Effect in Ferromagnetic Semiconductors

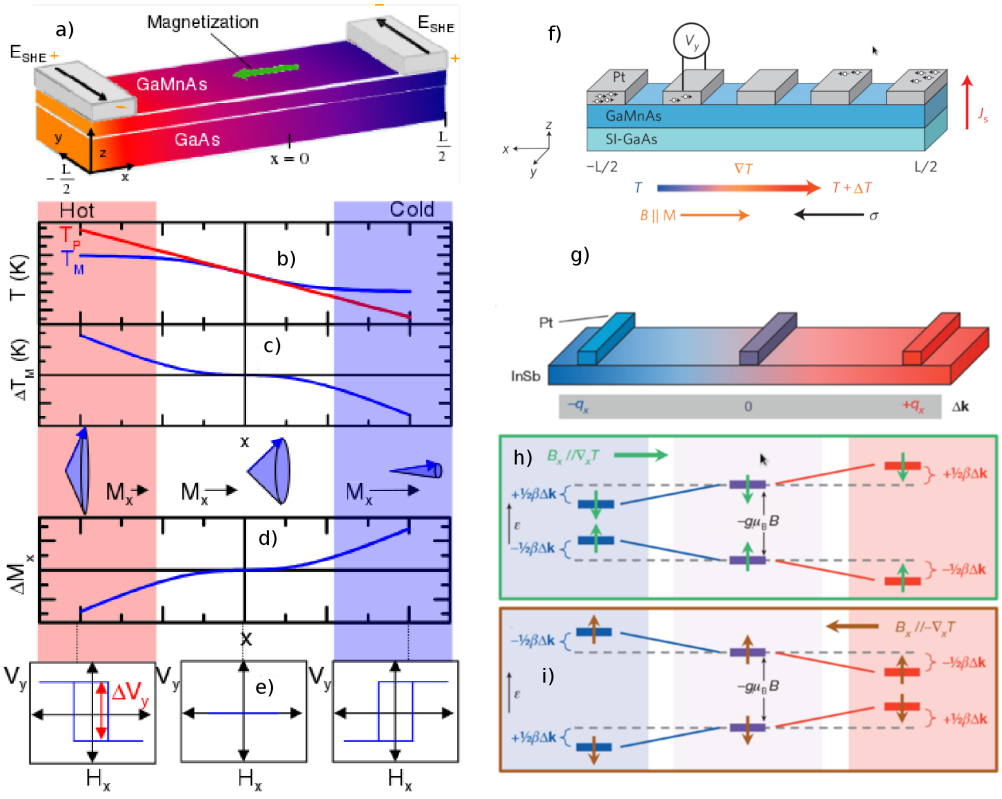

Figura 4.2: Spin Seebeck effect in Semiconductors. Figure taken from ref's [3], [4] and [5]

In 2010, Jaworski et al., reported the existence of SSE in the ferromagnetic semiconductor $Ga_{1-s}Mn_sAs$ grown on a (001) semi-insulating $GaAs$ [3]. This material

have interesting advantages, as, measure in the magnetic phase transition, large spin polarization and flexible design of $\vec{M}$ directions (this direction can be designed using epitaxial strain to have $\vec{M}$ in plane or out of plane). Here, the spatial distribution of the spins caused by the SSE follows a $Sinh(x)$ law, another important discovery was that even scratching the sample the effect remains, demonstrating that the SSE don't need charge/spin carriers. The geometrical configuration of the montage were identical to that of the TSSE and also used a Pt wire as spin current detector Fig4.2 f). The out of plane $\vec{M}$ configuration allow the measurement of the voltage due to the transverse Nernst-Ettingshausen effect that, in contrast with the SSE, don't change with the longitudinal position of the Pt wire on the sample, reaffirming that effectively exist the SSE. All measurements was made under the curie temperature T_c of each sample, the lower temperature was 40 K and the higher 165 K. The next year, the same group studied the FM semiconductor GaMnAs over an extended range of temperatures below T_c Fig. 4.2 a) [4]. Thus, was characterized the T-dependence of the spin Seebeck coefficient (S_{xy}), of $\vec{M}$ and of the TEP in the FM, alongside the specific heat and thermal conductivity of the substrate. The results give rise to the conclusion that the spin redistribution is driven by the phonons. Thus, they propose a phenomenological theory based on phonon-magnon drag (PMD). The Fig4.2 b) show the temperature profile of phonons and magnons and c) shows the difference, the change in the magnetization due to phonon drag across the temperature gradient appear in d) and hysteresis loops representing the transverse voltage detected on the Pt strips in each x position are schematized in e). In this works was observed that the SSE effect disappear when $T > T_c$ and the semiconductor is paramagnetic. The conventional order of magnitude of V_{ISHE} on the NM was a few μV.

Finally in 2012 it was reported a giant SSE with the values of V_{ISHE} on the order of mV. The samples were Te-doped InSb of the n-type Fig. 4.2 g), this system was selected because phonon-electron drag (PED), spin polarizability, and s-o coupling are maximized. The phenomenological proposed explanation, was that the effect is mediated by a large PED that modifies the Zeeman spin-splitting energy through the s-o interaction [5].

4.3 Spin Seebeck Effect in Ferromagnetic Insulators

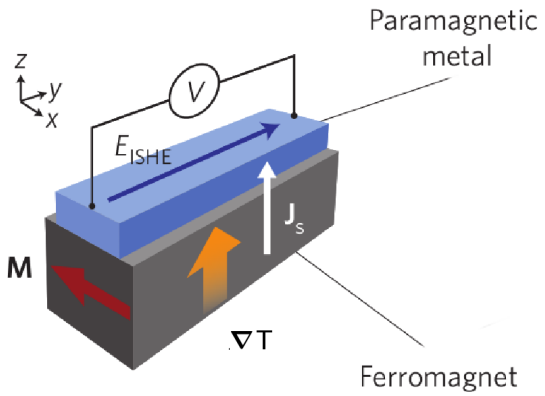

Figura 4.3: Longitudinal Spin Seebeck Effect configuration [Fig. 3 of ref [37]].

In 2010 K. Uchida et al., discovered the existence of the SSE in magnetic insulators, first in $LaY_2Fe_5O_{12}$ (La:YIG) [13], and then reported the existence of the SSE in a different geometrical configuration called Longitudinal (LSSE) in YIG/Pt samples. The geometry of the LSSE is shown in Fig. 4.3, where ∇T and J_s^p are parallel to each other [93]. They also reported the LSSE in poly-crystalline insulating magnets, such as $(Mn, Zn)Fe_2O_4$ [94]. To explore another samples 2012 K.Uchida et al., measured both geometrical configurations of SSE in Py/Pt, YIG/Pt and La:YIG/Pt [95], and also they studied LSSE in various garnet ferrites of the form: $Y_{3-x}R_xFe_{5-y}M_yO_{12}$ $(R = Gd, Ca; M = Al, Mn, V, In, Zr)$ [96], founding an improvement of the LSSE with the Fe concentration that corresponds to a change in $g^{\uparrow,\downarrow}$ of the interface with a Pt layer.

4.4 Recent Works on TSSE and LSSE in Metals and Insulators

Brief Review of works on Ferromagnetic Metals

The discovery of the SSE strengthened and motivated several works. In 2010 A. A. Tulapurkar and Y. Suzuki realized that a pure spin current can be generated with a ∇T, from the spin-dependent SE that should be distinguished from the SSE [78]. For the computation they solve the Boltzmann equation including electron-magnon scattering. Also was obtained the need temperature gradient to switch the magnetization of a nano-magnet by means of a spin current, being about $2.3K/nm$ at room temperature. This same year A. Slachter et al., reached the spin injection from a FM into a NM using the spin-dependent SE (not the SSE) with a non-local spin-valve in lateral geometry, instead of the perpendicular one [97]. The phenomena is an alternative to the electrical injection and is based on a heat current flowing at the FM/NM interface and not at the bulk. This was explained with a diffusive-transport theory.

In 2011 S. Bosu studied the SSE in the half-metallic Heusler compound Co_2MnSi [98]. This year, K. Uchida et al., discussed the long-range nature of the SSE, demonstrating that a Py/Pt bilayer is sensible to the position over a sapphire substrate which have an in-plane gradient [78]. In the same work they introduce the acoustic spin pumping, that is the generation of a spin current through the FM/NM interface with a sound wave excitation driven by the substrate, in this case the sample is YIG/Pt fixed to a piezoelectric actuator as lead-zirconate-titanate (PZT) ceramic. Another interesting feature of the SSE is that the effect of the substrates in the SSE measurements is very important, introducing asymmetries in the transverse and longitudinal thermal voltage with respect to the ∇T direction, this was realized first by S. Y. Huang et al., [99]. With this motivation they studied the intrinsic spin-dependent thermal transport on substrate-free samples, presenting angular dependence of the form $cos^2\theta$ where θ is the angle between $\vec{H}$ and ∇T.

In 2011 Marius V. Costache developed a device that contains a set of FM wires connected electrically in series and thermally in parallel [100]. The whole system is placed between a hot and a cold source. The control of the successive orientation of $\vec{M}$ in pairs of wires allow the independent study of the magnon drag and the

thermoelectric effects (electron and phonon drag) at low magnetic fields $\approx\ 0,1T$. Application of this magnon drag thermopile-like device to a NiFe demonstrates the existence of the magnon drag mechanism in this system.

Brief Review of Works on Ferromagnetic Insulators

T. Kikkawa et al., demonstrate that the LSSE in Au/YIG and $Pt/Cu/YIG$ exist even when the Anomalous Nernst Effect, brought by the proximity effect, is fully removed [101]. They concluded that the ANE contribution is negligibly small for the conventional YIG/Pt, the use of Cu and Au is because Au and Cu are far from the Stoner ferromagnetic instability. Maybe the most valuable feature of the existence of SSE in insulators is that conduction electrons are not necessary for the SSE, shown also that the SSE is a universal phenomenon for magnetic materials. Due to the existence of the Anomalous Nernst effect, the LSSE configuration, is practical specially for insulators. In the TSSE $\vec{M}$ and ∇T are collinear, then even in metals the TSSE is not distorted.

The discovery impulse several researches in the later years. In 2012 Lei Lu Yiyan Sun et al., using a GGG/YIG/Pt films achieve by the first time the control of FM relaxation with spin transfer induced thermally through the SSE, the process is detected measuring the line-width of the spin wave resonance [102] and the magnetization dynamics was measured by microwave detection. But secondary spin waves (SW) with much higher wave vectors can be excited by two magnon process, [103], [104] and the process contribute to the spin pumping, but is not detected by spin wave resonance, this motivate in 2013 M.B. Jungfleisch to make spin pumping measurements in YIG/Pt hetero-structures [105]. They introduce a method to identify, in the V_{ISHE}, SP from coherent magnons and SSE from incoherent magnons, and demonstrated that a spin pumping process in which a microwave drive the coherent magnetization precession, is accompanied by heating. These facts has been explored in the work of 2013 of T.An. [106], in which was realized that the excitation of a SW, at one side of a YIG strip, generate a heat flow heating the opposite end of the sample and that can be controlled magnetically. The SW/heat conversion is related to the damping, then using a YIG of low damping coefficients a remote heating was detected up to 10 mm away from the microwave excitation.

Björn Obry et al., in 2012 [107] studied the behavior of a coherent spin wave excited by microwaves on an magnetic insulator wave guide of YIG, presenting a continuously varying temperature, interestingly the local temperature is followed by a systematic variation of the spin wave wavelength, that is detected through phase-resolved Brillouin light scattering interference measurements. Was also saw that a forbidden spatial region is created by ∇T causing a reflection of the SW's. In this way [108] R. O. Cunha reported the action of the LSSE spin currents on the relaxation rate of the SW excited on a YIG/Pt system by microwave techniques. One of the remarkable results is that changes in damping were observed only with the presence of the Pt layer, the change depend of the sign of ∇T, amplifying or attenuating the SW. The Pt presence is need as a source and sink of angular momentum. The same year G. L. da Silva et al., [109], realized that an enhancement of the SW modes excited in YIG/Pt FMR experiments, is achieved with the application of ∇T, if the gradients is reversed the SW is attenuated. Theoretical studies in this phenomena was conducted by Sylvain D. Brechet et al., [110], who presented evidence for a magnetic Seebeck effect i.e. the induction of a magnetic field produced by SW in presence of a ∇T. They established a formalism for the irreversible thermodynamics governing a continuous medium with magnetization explaining how the modification of the Landau-Lifshitz equation generate contribution to the dissipation that is linear in ∇T. On the other way the name magneto-Seebeck effect was used to explain a change in the Seebeck coefficient due to the magnetic response of nanostructures [111]

5. RESULTS ON THE LSSE

For the study of the LSSE in hybrid structures we have carried out several measurements and a magnon spin current theory for the LSSE was developed to explain the experimental results, that are described in this chapter and then the analysis will be made in the chapter 6. We separate our measurements in those carried at room temperature, and the ones at low temperature for a better understanding.

5.1 LSSE at room temperature

5.1.1 Samples Details

For the LSSE study at room temperature, the FMI material is a pure single crystal YIG, and the NM material is a thin metallic layer of Pt, Py or Ta. The selection of these metals is because the Pt is known to have reasonably large values for the spin orbit interaction and $g^{\uparrow\downarrow}$ with YIG, being widely used in experiments involving ISHE, the Ta because was reported the existence of the giant ISHE in this system [47], and the Py because was detected the existence of ISHE in this ferromagnetic metal. The single crystals used in this chapter were prepared by Prof. Antonio Azevedo at Carnegie Mellon University by Liquid Phase Epitaxy ref [112]. The nanometric films deposited on the surfaces of the crystals were prepared by DC magnetron sputtering, the noble gas used to eject the atoms from the target was high purity argon (99.999%) and the vacuum chamber is prepared with ultrahigh vacuum $< 3 \times 10^{-7}$ torr, but after the Ar injection the pressure arise to $\approx 3 \times 10^{-3}$ torr. The deposition rate of our equipment is regularly calibrated using a profilometer, thus the thickness of the films is determined with the deposition time and is typically

a few nanometers per minute. The first set of samples consisted of three strips of single crystal YIG (111) film grown by liquid phase epitaxy onto a 0.5 -mm-thick [113]-oriented $Gd_3Ga_5O_12$ (GGG) substrate. Growth was made at a constant temperature in supersaturated solutions using a $PbO - B_2O_3$-based flux by the horizontal dipping technique. The strips are 7.0 mm long and 2.0 mm wide, and the YIG film is $6\,\mu m$ thick, with the thickness measured directly with a scanning electron microscope. Each YIG strips is covered respectively with a Pt (6 nm), Ta (2nm) or Py (10 nm) layer deposited by magnetron sputtering. To achieve the low temperature measurements, a second sample of YIG/Pt is prepared similarly to that above but with the dimensions 10.0 mm long, 2.3 mm wide, and the thickness of the YIG film being $8\,\mu m$.

Taking into account that the predicted magnon diffusion length for YIG is $26\,\mu m$, and with the aim of study the behavior of the LSSE with an abrupt change in the YIG layer thickness, we have also investigated a 1-mm-thick single-crystal YIG slab with the dimensions 10 mm length, 3 mm wide and 1 mm thick, cut with faces along (111) from a boule grown by the Czochralski method. The faces are optically polished, and one of them is fully covered with a 6-nm-thick Pt layer.

5.1.2 Home Made LSSE Measuring System

We characterized the existence and behavior of the LSSE at a constant base temperature, that we set at room temperature, and for all the five samples the following procedure was applied. We have used an arrangement similar to those of Uchida et al. [15, 16, 40] and Kikkawa et al. [41], as illustrated in Fig. 5.1 (a).

Here, the sample is placed between the poles of an electromagnet that produces a nearly homogeneous and uniform magnetic field H_0 at the sample position. A commercial Peltier module is used to heat or cool the metallic side of the bilayer, while the insulating side of the sample is in thermal contact with a copper block which is maintained at room temperature, using the metallic structure of the electromagnets and supports as a thermal bath Fig. 5.1 (b). In this configuration the temperature gradient ∇T is parallel to the pump spin current J_S^{sp}. Two Cu wires attached with silver paint to the ends of the metallic layer are used to measure the

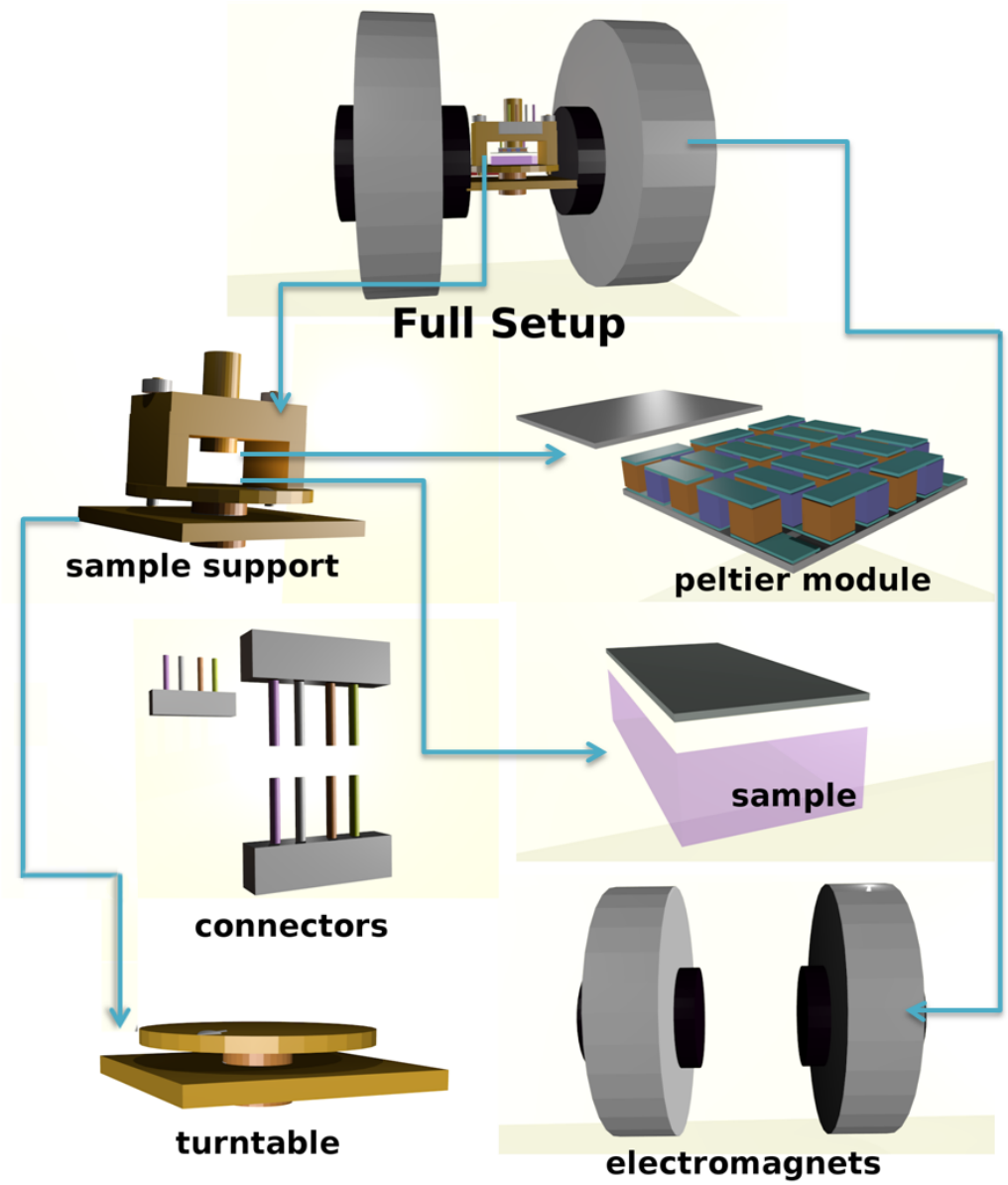

Figura 5.1: Homemade setup for the LSSE measurements.

dc ISHE voltage directly with a nanovoltmeter. The temperature difference across the sample is calibrated as a function of the current in the Peltier module by means of two thermocouples attached to thin copper sheets one placed between the Peltier

module and the sample and the other between the cooper block and the sample. We fabricated the support in a way that allowed us to study the angular dependence of the V_{ISHE} as a function of the angle between H_0 and J_c. This dependence eliminate discrepancies about the magnetic origin of the electric signals.

5.1.3 LSSE at Room Temperature Detected with Non-magnetic and Ferromagnetic Metals: Pt,Ta and Py

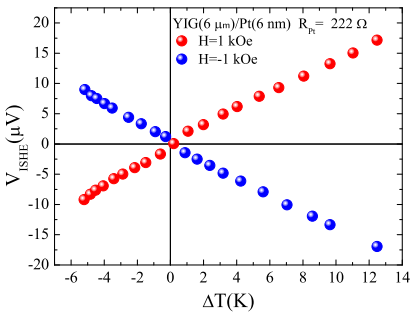

(a) $GGG/YIG(6\mu m)/Pt$

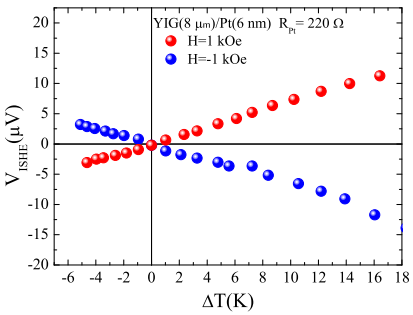

(b) $GGG/YIG(8\mu m)/Pt$

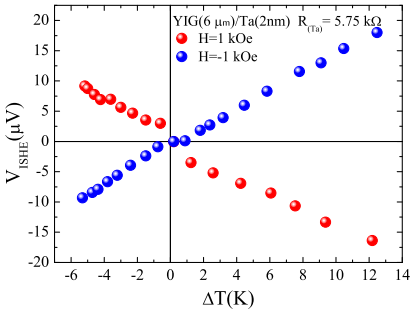

(c) $GGG/YIG/Ta$

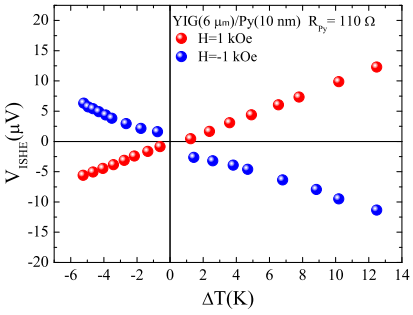

(d) $GGG/YIG/Py$

Figura 5.2: Variation of the dc ISHE voltage V created by the spin Seebeck effect with the temperature difference ΔT for $H = \pm 1.0\, kOe$.

The Fig. 5.2 shows the results of the measure V_{ISHE}, for the four samples with the YIG in film, setting the magnetic field at the constant value of $H = \pm 1.0\, kOe$ and varying the temperature difference from $\approx -6\ K$ to $\approx 12\, K$ the reason for the asymmetry in the ΔT values is that the cooler power of the Peltier module is decreased by the Joule heating when the electric current in it is greater than $0.5\ A$. We see that the sign of V_{ISHE} is inverted for the Ta with respect to the other metals, as the geometrical configuration is identical, we can conclude that the Θ_{SH} has opposite sign for this material. Although we expect large values for the signal from the YIG/Ta system, Fig. 5.2 (c) shows that the intensity of the signal is comparable with those of the YIG/Pt. The reason for this may be that the ISHE in our system is inside a thermal gradient and then the origin of the V_{ISHE} could be intrinsic and then do not depend on the sample resistance as the extrinsic Hall effects, that could be dominant in the experiments of ref. [48]. The FM Py effectively works well as ISHE detector as reported by Miao et al., . ref [114], although the signal is $\approx 35\%$ lower than those of Pt, this is caused because the resistance of the Py $R = 110\,\Omega$ is lower than those of the Pt $R_{Pt} = 208\,\Omega$. The high symmetry of the signals in Fig. 5.2 with respect to the temperature and field reversal is a clear evidence that the phenomenon has a thermomagnetic nature. Also as mentioned in chapter 4, T. Kikkawa et al., demonstrate that in YIG/Pt in the LSSE configuration, the anomalous Nernst effect contribution is negligibly small.

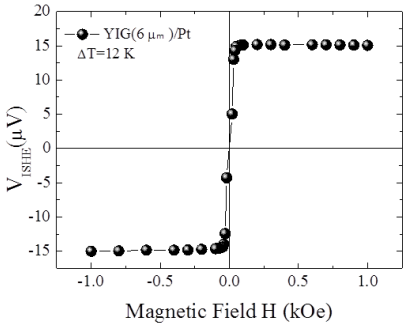

(a) $GGG/YIG(6\mu m)/Pt$

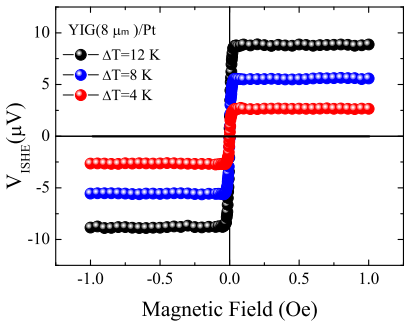

(b) $GGG/YIG(8\mu m)/Pt$

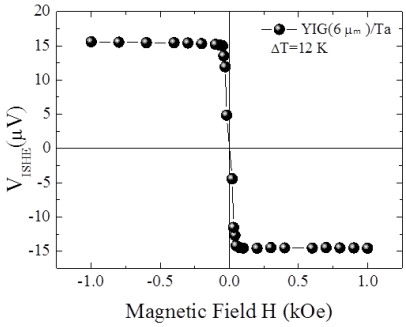

(c) $GGG/YIG(6\mu m)/Ta$

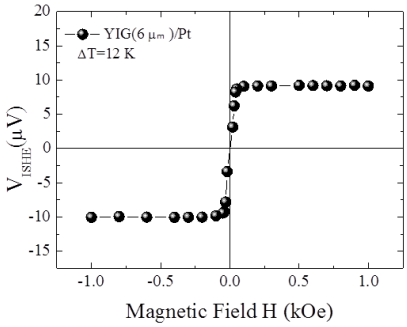

(d) $GGG/YIG(6\mu m)/Py$

Figura 5.3: Variation of the dc ISHE voltage V created by the spin Seebeck effect with the intensity of the magnetic field $\vec{H}$ for $\Delta T = \pm 12\ K$.

The magnetic field dependence of the LSSE for the same samples with a constant temperature difference of 12 K is shown in Fig. 5.3. It is verified that in the absence of the external magnetic field the signal disappear, and is activated progressively for a few Oe up to overcome the demagnetization energy. Over $\approx 50\ Oe$ the V_{ISHE} is constant with $\vec{H}$ and as expected, the signal for YIG/Ta has opposite polarization than the other systems. The Fig. 5.3 (b) shows the V_{ISHE} vs. $\vec{H}$ variation for three values of ΔT i.e. $4\,K$, $8\,K$ and $12\,K$. Thus, independently of the temperature,

the application of an external magnetic field is fundamental for the existence of the LSSE, and as the effect of ΔT is only to increase the saturation value of V_{ISHE}, but does not modify the shape of the curve. We argue that the V_{ISHE} arises totally from the effective pumped spin current in the interface. The change in the sign of the voltage with the reversal of the direction of the magnetic field is due to the change in the sign of the spin polarization, some of these results were included in ref. [115].

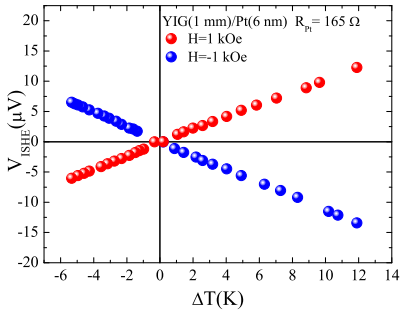

(a) $YIG(1mm)/Pt$

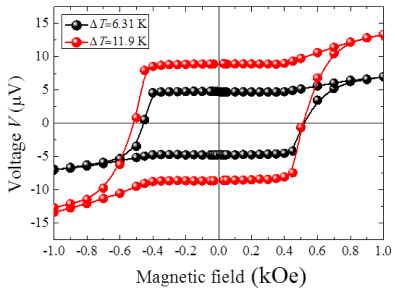

(b) $YIG(1mm)/Pt$

Figura 5.4: Variation of the dc ISHE voltage created by the spin Seebeck effect with (a) the temperature difference ΔT for $H = \pm 1.0\, kOe$ and (b) the intensity of the magnetic field $\vec{H}$ for $\Delta T = \pm 12\ K$.

For the case of the bulk system YIG(1mm)/Pt, the V_{ISHE} vs. ΔT and V_{ISHE} vs. $\vec{H}$ curves are shown respectively in figures 5.4 (a) and 5.4 (b), Figure 5.4 (a) is similar to those for the samples with $8-$ and $6-\mu m$-thick YIG. However Fig. 5.4 (b) presents a hysteresis-like loop not observed in the other samples. To explore the origin of this phenomenon, we take a measurement of V_{ISHE}, fixing ΔT and $\vec{H}$, and changing every 15 degrees the angle between the sample axes and the $\vec{H}$ direction the result is shown in Fig. 5.6. The expected situation considering the eq. 3.8 i.e. $\vec{J}_c = \Theta_{SH}\frac{2e}{\hbar}\vec{J}_s \times \hat{\sigma}$, is a maximum signal when the longitudinal axis of the sample and the magnetic field are parallel to each other and a null signal when are perpendicular. This behavior appears in all the other samples, but in the current one, the sinusoidal cycle is distorted appearing expanded between -90 and 45 and compressed between 45 and 90. In a first view it is a very strange dependence, then,

we make a measurement of the magnetization hysteresis loop for longitudinal and transversal axes (0 and 90 degrees) with a vibrating sample magnetometer as shown in Fig. 5.5. Here clearly the black curve shows that exists an anisotropy in the magnetization for the transverse field, the magnetization is saturated in $\approx 500\,Oe$ that is the approximately the same position for the remnant V_{ISHE} in Fig. 5.4 (b). These facts lead us to conclude that there exists a demagnetization energy coming from the shape factor that make the easy axis of magnetization rotate 45 degrees from the longitudinal axis of the sample. This was confirmed with carefully hanging the sample between the electromagnets with a thin thread. Varying the field intensity it was observed the orientation of the sample. For high fields the sample is oriented parallel to $\vec{H}$ but under $\approx 4\ Oe$ the sample axis stays 45 degrees rotated. Thus, we determined an unexpected feature of the LSSE/ISHE phenomenon that has to be considered when the FMI layer have bulk dimensions i.e. The shape anisotropy generates a strong remnant V_{ISHE}, remembering a hysteresis loop, although the eq. 3.8 has not to be modified, to satisfy a distorted angular dependence, we argue that being a bulk sample of YIG, the proximity effect came stronger and make σ feel the combined effect of the magnetization of the insulator and of the external magnetic field, so we have to take care in the interpretation of $\vec{\sigma}$ term in eq. 3.8 as the real spin polarization and not as the $\vec{H}$ direction. In fact the distortion in Fig. 5.6 together with eq. 3.8 could determine the spin polarization at each angular position.

Since the thicknesses of the Pt/YIG/GGG structures and of the Pt/YIG slab are 0.5 and 1.0 mm, respectively, for a given T , the temperature gradient ΔT is twice as large in the former in comparison with the latter. One important conclusion drawn from the data of figures 5.2 (a), (b) and 5.4 (a) is that the voltage due to the SSE spin current in an $6-\mu m$-thick YIG film is comparable to that in a 1-mm-thick YIG slab. In other words, for a fixed temperature gradient, V is nearly independent of the FMI layer thickness in the thickness range of the measurements.

5.2 LSSE at low temperatures

The LSSE measurements at room temperature shows that Pt is the most stable material to be used as ISHE sensor in the low temperature measurements. This is

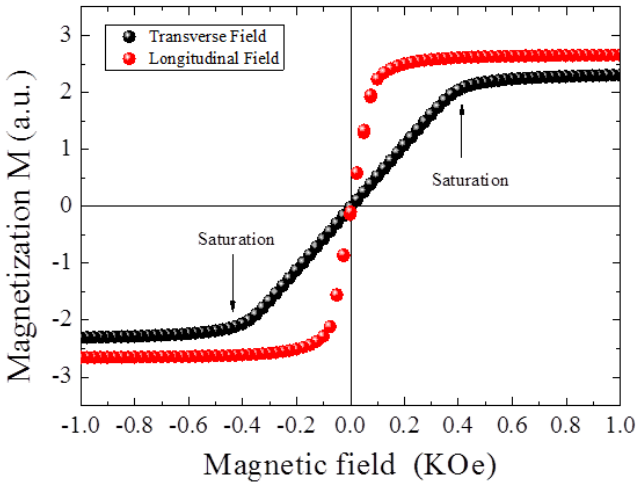

Figura 5.5: Magnetometer analysis for the YIG(1mm)/Pt sample. We consider transverse magnetic field when it is perpendicular to the longitudinal axis of the sample and longitudinal field for the parallel case, in both situations the field is applied in-plane.

in agreement with the fact that the Pt is known to have reasonably large values for the spin-Hall angle and spin mixing conductance with YIG. Actually, the samples with Py and Ta needed special care to avoid parasitic signals. Then, we selected the $YIG(8\mu m)/Pt$ system for investigate the low temperature features of the LSSE.

5.2.1 Measurement Technique: Displex Closed Cycle Cryostat

For the measurements of the V_{ISHE} as a function of the base sample temperature, The $YIG(8\mu m)/Pt$ system was mounted directly on the copper base of a Displex closed cycle cryostat, Fig. 5.7 and glued with General Electric varnish. The temperature gradient is created by heating the Pt side with a heater, made of a resistive wire in zigzag between two sheets of Kapton (polyimide), while the opposite GGG side is maintained at the base temperature T_b of the cryostat. The temperature difference ΔT across the Pt/YIG/GGG structure was measured with a Cu-constantan-Cu differential thermometer made of two thermocouple junctions,

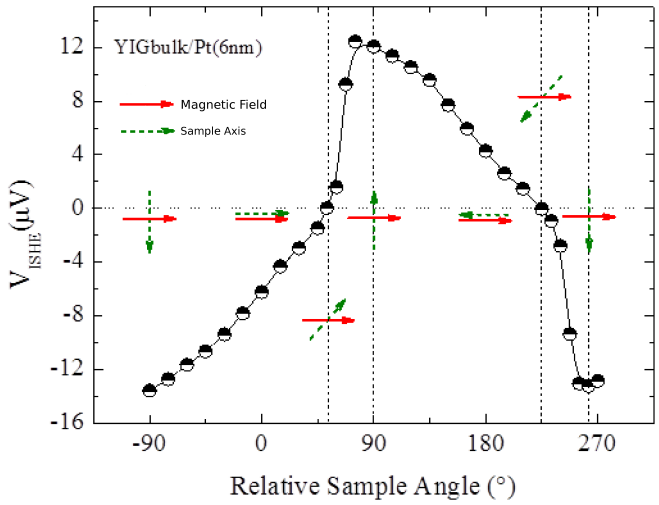

Figura 5.6: Angular dependence of the dc ISHE voltage generated in a Pt layer through the longitudinal spin Seebeck effect of a YIG slab with $\Delta T = 12\,K$ and $H = 1\,kOe$. The green and red arrows represent respectively the sample axes and the magnetic field direction

one in contact with a thin copper strip placed between the heater and the Pt layer and the other in contact with the base. The calibration curve of the thermocouple junctions is shown in Fig.5.8 and the calibration parameters are tabled in the appendix. The Pt/YIG temperature used to plot the data is $T = T_b + \Delta T$, where T_b is the cryostat base temperature. The ISHE voltage was measured with a nanovoltmeter by means of two Cu wires attached with silver paint to the ends of the Pt layer. The Cu wires were also used to measure the resistance R_N of the Pt layer as a function of temperature.

5.2.2 LSSE at Low Temperatures in YIG/Pt Bilayers

The measurements from the setup of the last section are represented in Fig. 5.9, the red and blue spheres are the ISHE voltage measured respectively fixing the value of ΔT to $3\,K$ and to $7\,K$ while the sample temperature is varying and a transverse magnetic field of $H = 1\,kOe$ is applied. The external circuits and

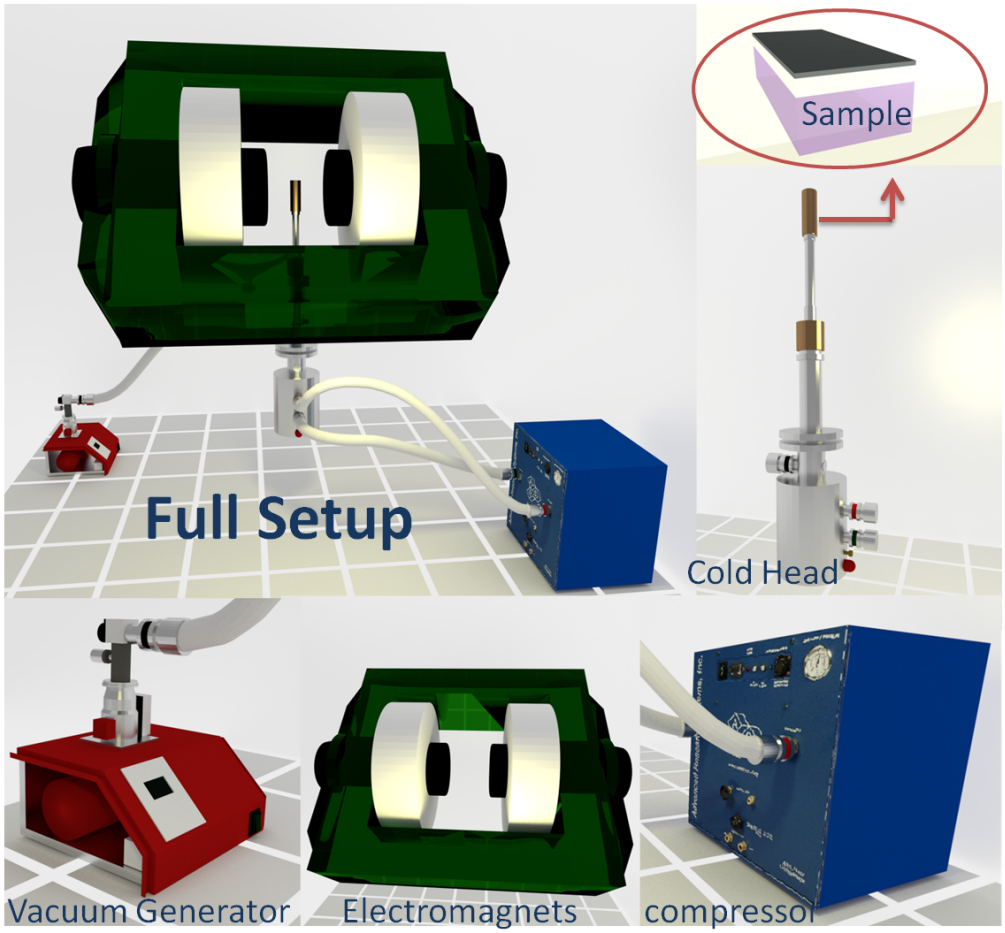

Figura 5.7: Displex closed cycle system

pickup give a residual contribution to the signal that was removed by subtracting the voltages measured with the fields in opposite directions. For the theoretical analysis of the LSSE, the resistance of the Pt layer was recorded for each temperature, the result is shown in the inset of Fig. 5.9 and the least-square fit reproduce $R_N(T) \approx R_N(300)[0.7+0.3(T/300)]$. The curves in Fig.5.9 were calculated with the theoretical model of the next chapter through Eq. 6.55. Thus the great agreement of with the experiments allow-us to validate our magnon spin current theory for the longitudinal spin Seebeck effect. The dotted lines represent the mechanism of interfacial thermal spin pumping falling off with temperature much faster than with the data.

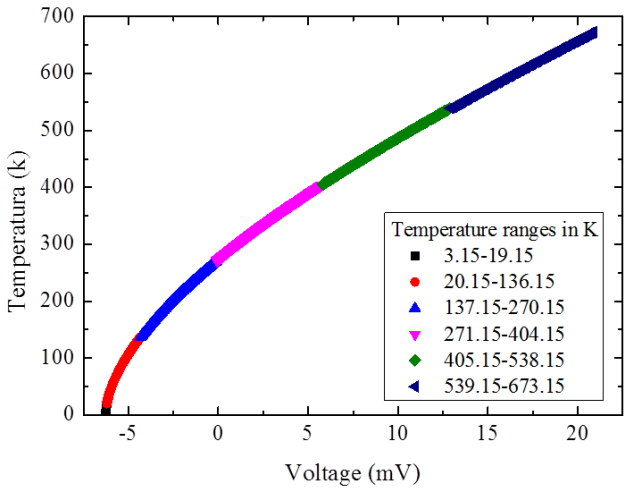

Figura 5.8: Calibration curve for the Cu-Constantan-Cu thermocouple.

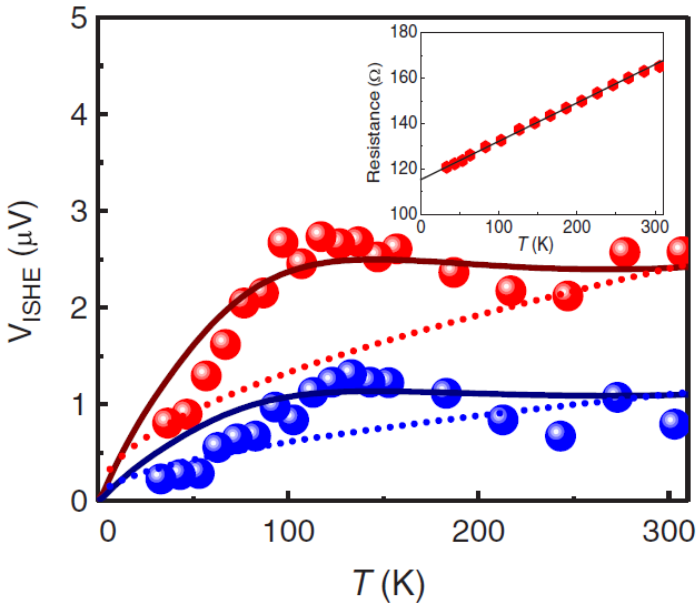

Figura 5.9: Comparison of the experimental data with calculated temperature dependence of ISHE voltage V created by the longitudinal spin Seebeck effect in yttrium iron garnet/platinum. The symbols represent the voltage measured with 3 K (blue) and 7 K (red). The dotted lines are calculated with the thermal spin pumping mechanism while the solid lines are calculated with the magnon spin current model presented here. The inset shows the measured resistance of the Pt layer and the linear fit used in the calculation of the voltage.(ref. [6])

6. ANALYSIS AND DISCUSSION

6.1 The Magnon Spin-Current Theory for the LSSE

For explaining the experimental results of the last chapter and in the lack of a satisfactory explanation for the LSSE, recently our group has proposed an alternative model for the origin of the LSSE published with some results of the current work in ref [6] . For the development of this theory, we have to consider an FMI/NM bilayer, Fig 6.1, in which we define the coordinate system in a way that the film lies in the x-z plane.

The sample is under the effect of a static and uniform external magnetic field $\vec{H}$ in the z direction, and a temperature gradient in the y axis, ∇T. The spin current inside a magnetic insulator is carried by magnons with a defined wave vector $\vec{k}$ and energy $\varepsilon_k = \hbar\omega_k$ [116, 117, 118, 119, 72], when the system is in equilibrium before thermal excitation the number of magnons is governed by the Bose-Einstein distribution as:

$$n_k^0 = \frac{1}{e^{\frac{\hbar\omega_k}{k_B T}} - 1}. \tag{6.1}$$

After excitation, the number of magnons is increased by $\delta n_k = n_k - n_k^0$ with n_k the actual number of magnons, the density of magnons, $\delta n_m = \delta n_k / V$, is also called

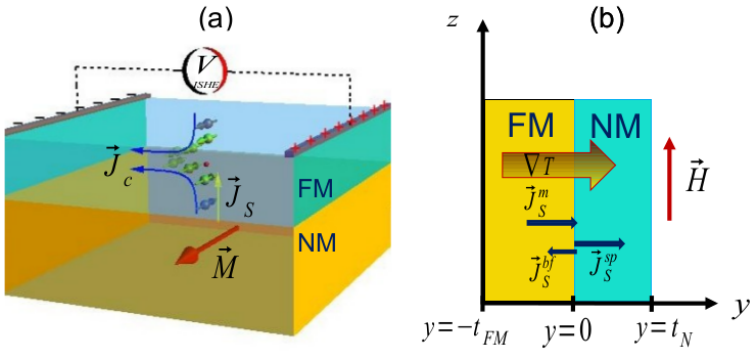

Figura 6.1: FMI/NM bilayer used to investigate the LSSE. (a) illustration of the conversion of the spin into the charge current by the ISHE in the NM layer. (b) Coordinate axes used to calculate the spin currents generated by a temperature gradient perpendicular to the plane of the bilayer.

magnon accumulation [116, 117], and can be expressed as:

$$\delta n_m = \frac{1}{V}\sum_k \delta n_k = \frac{1}{V}\sum_k (n_k - n_k^0),$$

or,

$$\delta n_m = \frac{1}{(2\pi)^3}\int d^3k \delta n_k = \frac{1}{(2\pi)^3}\int d^3k (n_k - n_k^0). \tag{6.2}$$

The collective spin precessions generate a magnetization current $\vec{J}_M^z$ and so a magnon spin current density $\vec{J}_S^z = \frac{\vec{J}_M^z}{\gamma}$, here γ is the gyro-magnetic ratio. Through a distribution function $f(\vec{k},\vec{r})$ we can write [116, 117]:

$$\vec{J}_S^z = \frac{\hbar}{V}\sum_k f(\vec{k},\vec{r})\vec{v}_k, \tag{6.3}$$

but in thermal equilibrium:

$$\sum_k f_0(\vec{k},\vec{r})\vec{v}_k = 0$$

$$\Rightarrow \ \vec{J}_S^z = \frac{\hbar}{V}\sum_k [f(\vec{k},\vec{r}) - f_0(\vec{k},\vec{r})]\vec{v}_k, \tag{6.4}$$

here $f(\vec{k},\vec{r}) = n_k$ and in integral form:

$$\vec{J}_S^z = \frac{\hbar}{(2\pi)^3}\int d^3k\vec{v}_k(n_k - n_k^0), \tag{6.5}$$

as this current is carried by pseudo-particles the transport caused by the thermal gradient obeys the Boltzmann equation:

$$\frac{f(\vec{k},\vec{r}) - f_0(\vec{k},\vec{r})}{\tau_k} + \vec{v}_k \cdot \nabla_r f(\vec{k},\vec{r}) + \frac{\vec{F}}{\hbar}\cdot\nabla_{\vec{k}} f(\vec{k},\vec{r}) = 0, \tag{6.6}$$

where τ_k is the k-magnon relaxation time. For n_k number and without external forces $\vec{F} = 0$ giving :

$$n_k(\vec{r}) - n_k^0 = -\tau_k\vec{v}_k \cdot \nabla n_k(\vec{r}) \tag{6.7}$$

or

$$n_k(\vec{r}) - n_k^0 = -\tau_k\vec{v}_k \cdot \nabla n_k^0(\vec{r}) - \tau_k\vec{v}_k \cdot \nabla[n_k(\vec{r}) - n_k^0(\vec{r})], \tag{6.8}$$

substitution in 6.5 gives:

$$\begin{aligned}\vec{J}_S^z = \frac{\hbar}{(2\pi)^3}\int d^3k\vec{v}_k\left(-\tau_k\vec{v}_k \cdot \nabla n_k^0(\vec{r}) - \tau_k\vec{v}_k \cdot \nabla[n_k(\vec{r}) - n_k^0(\vec{r})]\right)\\ = \vec{J}_{S\nabla T}^z + \vec{J}_{S\delta n}^z, .\end{aligned} \tag{6.9}$$

where we define the contributions of the temperature gradient and of the magnon accumulation as:

$$\begin{aligned}\vec{J}_{S\nabla T}^z &= -\frac{\hbar}{(2\pi)^3}\int d^3k\tau_k\frac{\partial n_k^0}{\partial T}\vec{v}_k(\vec{v}_k.\nabla T)\\ &\approx -\frac{\hbar}{(2\pi)^3}\sum_k \tau_k\frac{\partial n_k^0}{\partial T}\vec{v}_k\vec{v}_k.\nabla T,\end{aligned} \tag{6.10}$$

and:

$$\vec{J}^z_{S\delta n} = -\frac{\hbar}{(2\pi)^3}\int d^3k\tau_k\vec{v}_k(\vec{v}_k.\nabla\delta n_k(\vec{r})) \approx -\frac{\hbar}{(2\pi)^3}\sum_k \tau_k\vec{v}_k\vec{v}_k.\nabla\delta n_k(\vec{r}). \tag{6.11}$$

Eq.6.10 has the same form as the charge current that is generated from a Seebeck effect:

$$J^z_S = -S^z_S\nabla T = -S^z_S\frac{\partial T}{\partial y}. \tag{6.12}$$

With T, the average temperature that is the same for magnons and phonon systems [120], and using Eq.6.1 for $\frac{\partial n^0_k}{\partial T}$ with $x = \frac{\hbar\omega_k}{k_BT}$ we have:

$$S^z_S = \frac{\hbar}{(2\pi)^3T}\int d^3k\tau_k v^2_{ky}\frac{e^x x}{(e^x-1)^2}. \tag{6.13}$$

On the other hand Eq.6.11 give account of the nonuniform external means i.e. boundary conditions or temperature gradients. In the linear response theory n_k can be expanded as n^0_k plus a small deviation from the equilibrium in the form:

$$n_k(\vec{r}) = n^0_k + \frac{\partial n^0_k}{\partial\varepsilon_k}[\mu_m(y) + \sum_{n=1}^{\infty} g^{(n)}(y)P_n(cos\theta)] \tag{6.14}$$

where the chemical potential $\mu_m(y)$ is the $n = 0$ component of the small deviation and θ is the angle between $\vec{k}$ and the y axes. P_n is the Legendre polynomial of order n that satisfies the orthogonality relation:

$$\int_{-1}^{1} duP_{n'}(u)P_n(u) = \frac{2}{2n+1}\delta_{n,n'}. \tag{6.15}$$

With 6.14 and 6.15 in 6.2 we have:

$$\delta n_m = \frac{1}{(2\pi)^3}\int d^3k \frac{\partial n_k^0}{\partial \varepsilon_k}[\mu_m(y) + \sum_{n=1}^{\infty} g^{(n)}(y) P_n(cos\theta)] = \frac{1}{(2\pi)^3}\int d^3k \frac{\partial n_k^0}{\partial \varepsilon_k}\mu_m(y), \tag{6.16}$$

that can be written as:

$$\delta n_m(y) = I_0 \mu_m(y). \tag{6.17}$$

In a similar way we obtain:

$$J^z_{S\delta n(y)} = \frac{\hbar}{3} I_1 g^{(1)}(y), \tag{6.18}$$

with:

$$I_n = \frac{1}{(2\pi)^3}\int d^3k v_k^n \frac{\partial n_k^0}{\partial \varepsilon k}. \tag{6.19}$$

Refs. [116, 117] deduce a diffusion equation for the magnon accumulation:

$$\frac{\partial^2 \delta n_m(y)}{\delta y^2} = \frac{\delta n_m(y)}{l_m^2}, \tag{6.20}$$

that have the solutions:

$$\delta n_m(y) = A\cosh[\frac{(y + t_{FM})}{lm}] + B\sinh[(y + t_{FM})l_m], \tag{6.21}$$

where l_m is the diffusion length. They also shown that $J^z_{S\delta n(y)}$ is given by:

$$J^z_{S\delta n}(y) = \hbar D_m \frac{\partial}{\partial y}\delta n_m(y), \tag{6.22}$$

where the diffusion parameter is:

$$D_m = \frac{\tau_m I_2}{3 I_0} \tag{6.23}$$

and:

$$l_m = (D_m \tau_{SL})^{\frac{1}{2}}. \tag{6.24}$$

Substitution of 6.21 in 6.22 get:

$$J^z_{S\delta n}(y) = \hbar\frac{D_m}{l_m}A\sinh\left[\frac{(y+t_{FM})}{l_m}\right] + \hbar\frac{D_m}{l_m}B\cosh\left[\frac{(y+t_{FM})}{l_m}\right]. \tag{6.25}$$

Thus from 6.9 the total y component of the z-polarized magnon spin current density in the FMI is:

$$J^m_S(y) = -S^z_S\nabla_y T + \hbar\frac{D_m}{l_m}A\sinh\left[\frac{(y+t_{FM})}{l_m}\right] + \hbar\frac{D_m}{l_m}B\cosh\left[\frac{(y+t_{FM})}{l_m}\right]. \tag{6.26}$$

When $J^m_S(y)$ reach the FMI/NM interface a spin pumping process exist and the magnetic moment pass to be carried by the conduction electrons of the NM, the spin current pumped is [22, 121]:

$$\vec{J}^{sp}_S(0^+) = \frac{(\hbar g_r^{\uparrow\downarrow})}{4\pi M^2}\left(\vec{M}\times\frac{\partial\vec{M}}{\partial t}\right), \tag{6.27}$$

being $g_r^{\uparrow\downarrow}$ the real part of the spin mixing conductance. As the NM layer is of a few nanometers, part of the spin current reach the boundary and generate a backflow spin current J^{bf}_s that is injected into the FMI, decreasing the effective $\vec{J}^{sp}_S$. The spin current is polarized in the z-direction, then:

$$\left(\vec{M}\times\frac{\partial\vec{M}}{\partial t}\right) = \sum_k m^k_x\frac{dm^{-k}_y}{dt} - m^k_y\frac{dm^{-k}_x}{dt}. \tag{6.28}$$

With the L-L equation for each k-mode is obtained:

$$\frac{dm_x}{dt} = \gamma H_z m_y = \omega_k m_y \tag{6.29}$$

$$\frac{dm_y}{dt} = -\gamma H_z m_x = -\omega_k m_x, \tag{6.30}$$

then:

$$\left(\vec{M}\times\frac{\partial\vec{M}}{\partial t}\right) = \sum_k \omega_k(m^2_x - m^2_y) = \sum_k \omega_k(m^+_k m^-_k), \tag{6.31}$$

where we use the circular polarized transverse components of the magnetization associated with the magnon k:

$$\begin{aligned} m^+ = m_x + im_y \qquad & and \qquad m^- = m_x - im_y \\ \Rightarrow m_x = \frac{m^+ + m^-}{2} \qquad & and \qquad m_y = \frac{m^+ - m^-}{2i}. \end{aligned} \tag{6.32}$$

With 6.31 on 6.27:

$$\vec{J}_S^{sp}(0^+) = \frac{\hbar g_{eff}^{\uparrow\downarrow}}{4\pi M^2} \sum_k \omega_k (m_k^+ m_k^-), \tag{6.33}$$

here $g_{eff}^{\uparrow\downarrow}$ is the real part of the effective spin mixing conductance that include the effects of the spin pumped as well as the backflow spin currents. Considering the linear approximation:

$$m_k^+ m_k^- = m_x^2 - m_y^2 = M^2 - M_z^2 \approx 2M(M - M_z) = \frac{2M\hbar\gamma\delta n_k}{V}, \tag{6.34}$$

6.33 can be expressed by:

$$\vec{J}_S^{sp}(0^+) = \frac{\gamma\hbar^2 g_{eff}^{\uparrow\downarrow}}{2\pi MV} \sum_k \omega_k \delta n_k \quad or \quad J_S^z(0^+) = -\frac{\gamma\hbar^2 g_{eff}^{\uparrow\downarrow}}{2\pi M} \frac{1}{(2\pi)^3} \int d^3k \omega_k \delta n_k. \tag{6.35}$$

As in 6.16:

$$J_S^z(0^+) = -\frac{\gamma\hbar^2 g_{eff}^{\uparrow\downarrow}}{2\pi M} \frac{1}{(2\pi)^3} \int d^3k \omega_k \frac{\partial n_k^0}{\partial E_k} [\mu_m(0)], \tag{6.36}$$

$$\tag{6.37}$$

using 6.17

$$J_S^z(0^+) = -\frac{\gamma\hbar^2 g_{eff}^{\uparrow\downarrow}}{2\pi M} \frac{1}{(2\pi)^3} \frac{\delta n_m(0)}{I_0} \int d^3k \omega_k \frac{\partial n_k^0}{\partial E_k}, \tag{6.38}$$

$$\tag{6.39}$$

with $x \equiv \hbar\omega_k / k_B T$ and 6.1:

$$\frac{\partial n_k^0}{\partial E_k} = \frac{1}{k_B T}\frac{\partial n_k^0}{\partial x} = -\frac{e^x}{(e^x-1)^2}\frac{1}{k_B T} \tag{6.40}$$

$$\tag{6.41}$$

and so:

$$J_S^z(0^+) = -\frac{\gamma\hbar g_{eff}^{\uparrow\downarrow}}{2\pi M}\frac{1}{(2\pi)^3}\frac{\delta n_m(0)}{I_0}\int d^3k\hbar\omega_k\left(-\frac{e^x}{(e^x-1)^2}\frac{1}{k_B T}\right) \tag{6.42}$$

$$= -\frac{\gamma\hbar g_{eff}^{\uparrow\downarrow}}{2\pi M}\frac{\delta n_m(0)}{((2\pi)^3 I_0)}\int d^3k\left(-\frac{e^x}{(e^x-1)^2}\frac{\hbar\omega_k}{k_B T}\right) \tag{6.43}$$

$$= -\frac{\gamma\hbar g_{eff}^{\uparrow\downarrow}}{2\pi M}\delta n_m(0) k_B T\frac{C_1}{C_0}, \tag{6.44}$$

where we did:

$$C_1 = \int d^3k\frac{xe^x}{(e^x-1)^2} \qquad and \qquad C_0 = \int d^3k\frac{e^x}{(e^x-1)^2}. \tag{6.45}$$

Eq. 6.44 relates the spin current in the NM to the magnon accumulation at the interface. The next step is to find the coefficients of 6.21, and the magnon accumulation at the FMI/NM interface $\delta n_m(0)$, in terms of the thermal gradient ∇T. The conservation of angular momentum flow on the boundaries require the continuity of the spin currents at the interfaces [116, 117, 22, 121, 122]. Based on the figure 6.1:

$$J_s^z(y = -t_{FM}) = 0, \tag{6.46}$$

$$and$$

$$J_s^z(y = 0^-) = J_s^z(y = 0^+). \tag{6.47}$$

$$\tag{6.48}$$

Through 6.46 in 6.26 we have:

$$B = \frac{S_s^z l_m}{\hbar D_m}\nabla T. \tag{6.49}$$

With substitution in Eq. 6.21:

$$A = \frac{\delta n_m(0)}{\cosh \frac{t_{FM}}{l_m}} - \frac{S_s^z \nabla T l_m}{\hbar D_m} \tanh\left(\frac{t_{FM}}{l_m}\right) \tag{6.50}$$

and through 6.47 together with Equations 6.26 and 6.44:

$$\delta n_m(0) = \frac{1 - \cosh^{-1}\left(\frac{t_{FM}}{l_m}\right)}{a \tanh\left(\frac{t_{FM}}{l_m}\right) + b g_{eff}^{\uparrow\downarrow}} S_S^z \nabla T, \tag{6.51}$$

where:

$$a = \hbar \frac{D_m}{l_m} \qquad \textit{and} \qquad b = \frac{\gamma \hbar k B T C_1}{2\pi M C_0}. \tag{6.52}$$

When the condition $a >> b g_{\uparrow,\downarrow}$ is satisfied, as in the YIG ferrimagnet, then:

$$J_S^z(0) = -\frac{b g_{eff}^{\uparrow\downarrow} \rho}{a} S_S^z \nabla T. \tag{6.53}$$

So, we have clearly shown that the generated spin current depends not only of ∇T, but explicitly also of $g_{eff}^{\uparrow\downarrow}$, this result shows that the NM layer in contact with the FMI film is essential for the existence of the spin current, explaining the experimental fact that a Pt layer in contact with films of YIG is necessary for using the SSE to control the relaxation rate of the magnons in the YIG [102, 105, 108].

In 6.53, ρ is a layer thickness parameter given by:

$$\rho = \frac{\cosh\left(\frac{t_{FM}}{l_m}\right) - 1}{\sinh\left(\frac{t_{FM}}{l_m}\right)}, \tag{6.54}$$

thus, for $t_{FM} >> l_m$, $\rho \approx 1$ and for $t_{FM} << l_m$, $\rho \approx 0$. Once the spin current is pumped on the NM will exist a transverse transformation on a charge current as $J_c = \Theta_{SH} \frac{2e}{\hbar} \vec{J}_S^z \times \vec{\sigma}$, explained in the chapter 3 [36]. With the actual geometrical configuration, J_c is between the ends of the NM layer, if R_N, t_N and w are the resistance, thickness, and width of the NM strip, integrating J_c along x and y is obtained:

$$V = R_N \omega \lambda_N \frac{2e}{\hbar} \Theta_{SH} \tanh\left(\frac{t_N}{2\lambda_N}\right) J_S^z(0). \tag{6.55}$$

Equation 6.55 is the measured voltage of Fig. 5.9, so using the correct parameters is possible to fit the experimental data and test the theory as will be shown in the next section.

6.2 Testing The Magnon Spin-Current Theory for the LSSE

At this point where we have an analytic expression for V_{ISHE} we need to find the appropriate form of 6.55 for the YIG($8\mu m$)/Pt system. The missing parameter of 6.55 is $J_S^z(0)$ given by eq. 6.53 that depends of S_S^z eq. 6.13 ,which is an integral in $\vec{k}$, and b eq. 6.52 that include the value of the integral C_1, eq. 6.45. Thus, our problem is reduced to calculate these integrals through a dispersion relation between the spin-wave angular frequency ω_k and the wave number k. Fig. 6.2 shows how the common quadratic dispersion relation of eq. 2.19 overestimate ω_k for high values of $\vec{k}$, as our experiments include magnons on the extreme of the Brillouin zone, is expected to Eq. 2.19 overestimate the value of V_{ISHE}. We obtain from Eq. 6.13:

$$S_S^Z = C_{5/2} \frac{k_B^{5/2} T^{3/2\tau_m}}{6\pi^2 \hbar^{3/2} (\gamma D)^{1/2}}, \tag{6.56}$$

where $C_{5/2}$ is a parameter given by

$$C_{5/2} = \int \frac{e^x}{(e^x - 1)^2} x (x - x_0)^{\frac{3}{2}} dx, \tag{6.57}$$

where $x_0 = \hbar\omega_0 / k_B T$. The lower limit of integration is x_0 , the minimum normalized spin-wave energy, determined by the magnetic field. The upper limit is the maximum energy at the Brillouin zone boundary. If we set $x_0 = 0$ and consider the upper limit infinity, since the integrand vanishes for large values of x, it can be shown that:

$$C_{5/2} = \Gamma(7/2)\zeta(5/2) \approx 4.46, \tag{6.58}$$

where $\Gamma(z)$ and $\zeta(z)$ are the gamma and Riemann zeta functions, respectively.

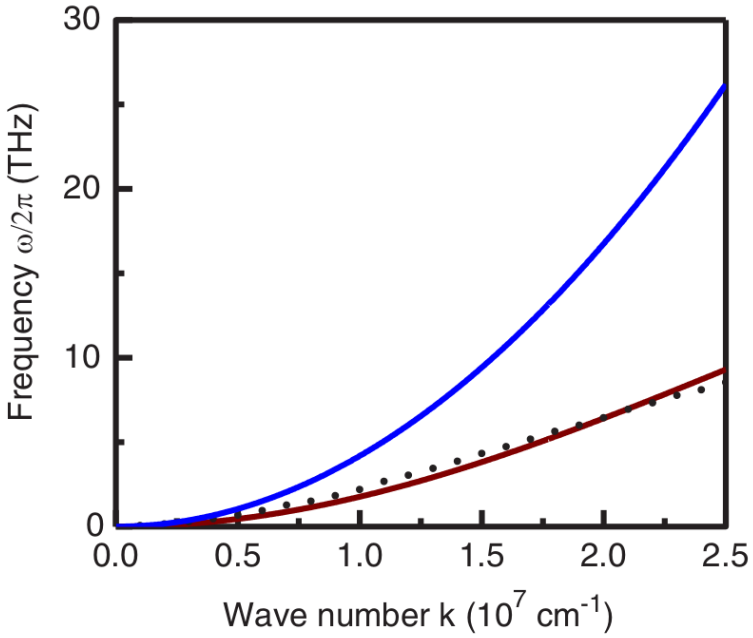

Figura 6.2: Spin-wave dispersion in YIG. The upper (blue) solid curve is calculated with quadratic dispersion. The dotted curve is calculated by Ref. [7] for k along a [111] direction. The lower (wine) solid curve is calculated with the linear approximation used to calculate the integrals. Figure from ref. [6]

For fields up to a few kOe, x_0 is small and the numerical integration of Eq. 6.14 gives a value close to the ones above. One can show that with the quadratic dispersion relation, the diffusion parameter in Eq. 6.23 becomes

$$D_m = \frac{4\tau_m k_B T \gamma D C_{3/2}}{3\hbar C_{1/2}}, \tag{6.59}$$

where

$$C_{1/2} = \int dx \frac{e^x (x - x_0)^{\frac{1}{2}}}{(e^x - 1)^2} \tag{6.60}$$

and

$$C_{3/2} = \int dx \frac{e^x (x - x_0)^{\frac{3}{2}}}{(e^x - 1)^2}. \tag{6.61}$$

If we set x_0 and consider the upper limit infinity it can be shown that:

$$C_{3/2} = \Gamma(5/2)\zeta(3/2) \approx 3.4. \tag{6.62}$$

For $x_0 \neq 0$, numerical integration shows that this value changes little for fields of a few kOe. The situation is different for $C_{1/2}$, because the integration diverges for $x_0 = 0$. Considering $H = 100\,Oe$, $x_0 = 4.2 \times 10^{-5}$, numerical integration gives $C_{1/2} \approx 250$. Using:

$$\begin{aligned} a &= \hbar(\frac{D_m}{\tau_{SL}})^{\frac{1}{2}}, \\ b &= \frac{\gamma \hbar k_B T C_{3/2}}{2\pi M C_{1/2}}, \end{aligned} \tag{6.63}$$

and S_S^Z given by Eq. 6.56, the spin current at the interface in Eq. 6.53 becomes, for $\rho = 1$,

$$J_S^z(0) = \frac{(k_B T)^2 (3\tau_{SL}\tau_m)^{\frac{1}{2}}}{4\pi M D 6\pi^2 \hbar} \left(\frac{C_{3/2}}{C_{1/2}}\right)^{\frac{1}{2}} C_{5/2} g_{eff}^{\uparrow\downarrow} k_B \nabla T. \tag{6.64}$$

Here, we introduce the parameters corresponding to YIG found in ref. [123]: $\gamma = 1.76 \times 10^7\, s^{-1}$, $D = 5.4 \times 10^{-9}\, Oe\, cm^2$,$4\pi M = 1.76\, kG$, $\tau_{SL} \approx 10^{-6}\, s$, and $\tau_m \approx 10^{-10}\, s$, which is an approximate average value for the magnon lifetime as calculated in the [6].

The reported [72, 82, 83, 74, 75, 76] values for the spin mixing conductance $g_{eff}^{\uparrow\downarrow}$ in YIG/Pt vary from $2 \times 10^{12}\, cm^{-2}$ to $4 \times 10^{14}\, cm^{-2}$. Considering $g_{eff}^{\uparrow\downarrow} = 10^{14}\, cm^{-2}$, we find from Eq.6.64 for $\Delta T = 300\, K/cm$ and $T = 300\, K$ a spin current density at the interface $J_S(0) \approx 10^{-4} erg/cm^2$. Using for Pt [65, 74, 75, 76, 84, 85, 86, 87] $\lambda_N = 4\, nm$, $\Theta_{SH} = 0.08$, and conductivity $\sigma_{Pt} = 2.4 \times 10^4 \Omega^{-1} cm^{-1}$, the resistance of a Pt strip with typical dimensions $l = 0.6\, cm$, $\omega = 0.2\, cm$, and $t_N = 6\, nm$ is $R_N = 208\, \Omega$, and we obtain from Eq. 6.55 an ISHE voltage of $V \approx 40 mV$. This is

more than three orders of magnitude larger than the experimental values of chapter 5 and of ref's. [15, 16, 40]. So as expected we need a more suitable form of $\omega_k(k)$. Then we use for the magnon dispersion relation [6] the form:

$$\omega_k = \omega_{ZB}\left(1 - cos\frac{\pi k}{2k_m}\right), \tag{6.65}$$

where ω_{ZB} is the zone boundary frequency and k_m is the value of the maximum wave number. Eq.6.65 was also plotted in Fig.6.2. being a better approximation for the magnon dispersion over the whole Brillouin zone. Also, we take into account that the magnon lifetime is a strong function of the wave number [6]. With the dispersion in Eq.6.65. The group velocity becomes:

$$v_k = \frac{\omega_{ZB}\pi}{2k_m} sin\frac{\pi k}{2k_m}. \tag{6.66}$$

Writing the magnon lifetime as $\tau_k = \tau_0/\eta_q$, where τ_0 is the lifetime of magnons near the zone center ($k \approx 0$) and $\eta_q q = \eta_k/\eta_0$ is an adimensional relaxation rate, Eq. 6.13 leads to

$$S_S^z = \frac{\hbar\tau_0 k_m \omega_{ZB}^2}{24T} B_S,$$
$$BS = \int_0^1 dq\, q^2 sin^2\left(\frac{\pi q}{2}\right)\frac{e^x}{\eta_q(e^x-1)^2}, \tag{6.67}$$

where $q = k/k_m$ is a normalized wave number. In Eq. 6.67, we consider spherical energy surfaces and integrate over a sphere of radius $km = \sqrt{3} \times 2.5/a_l$, a_l being the lattice parameter. One can show that with the dispersion relation in Eq. 6.65 and the wave number-dependent magnon relaxation rate, the diffusion coefficient in Eq. 6.23 becomes:

$$D_m = \frac{\tau_0 \pi^2 \omega_{ZB}^2}{12k_m^2}\frac{B2}{B0} \tag{6.68}$$

while the parameters in Eq. 6.52 are:

$$a = \frac{\hbar\tau_0\pi^2\omega_{ZB}^2}{12k_m^2 l_m}\frac{B2}{B0} and b = \frac{\gamma\hbar k_B T}{2\pi M}\frac{B1}{B0}, \tag{6.69}$$

where

$$B_0 = \int_{q0}^{1} dq q^2 \frac{e^x}{(e^x-1)^2}, B_1 = \int_0^1 dq\, q^2 \frac{x e^x}{(e^x-1)^2} \tag{6.70}$$

and

$$B_2 = \int_0^1 dq\, q^2 sin^2\left(\frac{\pi q}{2}\right) \frac{e^x}{\eta_q (e^x-1)^2}. \tag{6.71}$$

Using Eqs. 6.67–6.71 in Eq. 6.53, we obtain the following expression for the spin-current density at the FMI/NM interface:

$$J_S^z(0) = -\frac{\gamma \hbar \rho k_m^3 l_m}{4\pi M \pi^2} \frac{B_1 B_S}{B_2} g_{eff}^{\uparrow\downarrow} k_B \nabla T. \tag{6.72}$$

The integrals in Eqs. 6.67, 6.70, and 6.71 were evaluated numerically for YIG with the dispersion relation in Eq. 6.65, where $x = \omega_k/(k_B T)$, with $\omega_{ZB} = 6 \times 10^{13}\, s^{-1}$, corresponding to the zone boundary frequency of $9.5\, THz$ in Fig.6.2. In the integral in B_0 , we consider a minimum normalized wave number $q_0 = 10^{-3}$ determined by the boundary conditions imposed by the contact with the Pt layer [124]. We also use for YIG a lattice parameter $a_l = 1.23\, nm$, which gives $km = 2 \times 10^7 cm^{-1}$, and the normalized magnon relaxation rate due to 3- and 4-magnon processes:

$$\eta_q = \frac{\eta_k}{\eta_0} = 1 + (0.5q + 5.1q^2 - 3.25q^3) \times 10^3. \tag{6.73}$$

Hence, we find for $T = 300\, K$, $B_S = 2.2 \times 10^{-4}$, $B_0 = 282$, $B1 = 0.55$, and $B_2 = 5.1 \times 10^{-3}$. With these values and $\tau 0 = 0.5 \times 10^{-7}\, s$, we obtain a diffusion coefficient $Dm = 6.6\, cm^2/s$. Considering [117] $\tau_{SL} = 10^{-6}\, s$, we find from Eq. 6.23 a magnon diffusion length $l_m = 26 \mu m$. The use of all these parameter give a V_{ISHE} of a few μV, as shown in the fits of Fig. 5.9. so we have used the current analysis to fit the experimental results where we have considered also that the magnon relaxation rate varies with T^2 and that the magnetization depends of the temperature through:

$$M(T)/M(0) = 1.0 - 0.3(T/300)^2, \tag{6.74}$$

which represents well the experimental data for YIG [125]. In both cases, the magnon spin current vanishes at $T = 0$ because the thermal magnon population vanishes.

Since the magnon population decreases, whereas the lifetime increases, as T is lowered, the competition between the two factors results in the peak 30 K, which is a characteristic feature of our model. As will be shown later, the temperature dependence of the Pt layer resistance attenuates the peak somewhat.

An important signature of a theoretical model for transport phenomena is the temperature dependence of physical quantities of interest. Figure 6.4 shows curves for the temperature dependence of the spin currents calculated with various models relative to their values at $T = 300\,K$. The lower solid curve (wine) corresponds to Eq. 6.64 calculated with the quadratic dispersion relation and setting infinity for the upper limits of the integrals. In this case, the parameters in Eqs. 6.57 and 6.60 do not depend on the temperature and the spin current varies with T^2. The solid curve in the middle (red) represents a $T^{1/2}$ dependence, which applies to the mechanism of interfacial thermal spin current, Eqs. (12) and (15) of Ref. [10], that was used to interpret the experimental data obtained with transverse SSE in FMI layers.

The results of the calculation with Eq. 6.72, considering that $l_m \alpha D_m$, as in Eq. 6.23, are plotted in two ways: (1) the dotted curve (blue) is obtained assuming that the magnon relaxation does not vary with temperature, and (2) the upper solid curve (blue) was calculated considering that the magnon relaxation rate varies with T^2 [6], and the temperature dependence of the magnetization, given by $M(T)/M(0) = 1.0 - 0.3(T/300)^2$, which represents well the experimental data for YIG [125].

The linear dependence of V on T of Fig. 5.2 is well explained by Eqs. 6.55 and 6.72.Also the data of Fig. 5.3 show that for a fixed field direction, V does not depend on the value of the magnetic field, in agreement with the model. The result of different YIG thickens for the systems of YIG/Pt 5.2 (a), (b) and Fig. 5.4 seems to contradict the predictions of the model in Eq. 6.72, since sample A has $t_{FM} << l_m$ and the factor expressing the influence of FMI thickness in Eq. 6.54 is $\rho << 1$, while sample B has $t_{FM} >> l_m$ and consequently $\rho \approx 1$. However, we can see the Figure 6.3 that shows the data of Ref. [9] for the LSSE measured by the ISHE voltage in three series of YIG/Pt bilayers with varying YIG thickness normalized to the corresponding values at large thicknesses. This normalized quantity corresponds precisely to the thickness factor ρ of our model. We have used the same symbol to

represent the data obtained with the three series of sample. The solid line in Fig. 5 represents a least-square deviation fit of Eq. 6.54 to the data, which yields a magnon diffusion length lm = 70 nm.

The possible explanation for this small diffusion length compared to the one calculated before with Eq. 6.16 is that its relation with the diffusion coefficient should involve the magnon lifetime and not the spin-lattice relaxation time. In fact, with $l_m = 70\,nm$ and $D_m = 6.6\,cm^2/s$, we obtain $l_m^2/D_m \approx 0.7 \times 10^{-10}\,s$, which is on the same order of magnitude of the averaged magnon lifetime.

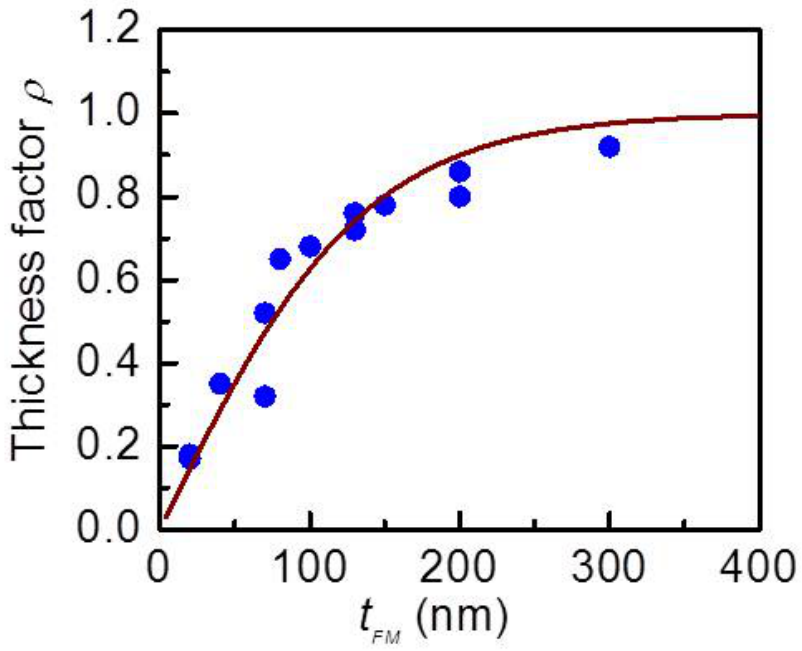

Figura 6.3: Symbols represent data of Ref. [8, 9] for the normalized LSSE for three series of YIG($t_F M$)/Pt bilayers. The solid line is a least-square deviation fit with Eq. 6.54.

Now we can use Eq. 6.72 to calculate the spin-current density created by a given temperature difference ΔT across a YIG/Pt bilayer. For $T = 15\,K$ in a sample that is 0.5 mm thick, the temperature gradient is $\Delta T = 300K/cm$. Using $l_m = 70\,nm$, $k_m = 2 \times 10^7\,cm^{-1}$, $B_S = 2.2 \times 10^{-4}$, $B1 = 0.55$, $B2 = 5.1 \times 10^{-3}$, $4\pi M = 1.76kG$, $\gamma = 1.76 \times 10^7 s^1 Oe^{-1}$, and $g_{eff}^{\uparrow,\downarrow} = 2 \times 10^{14}\,cm^{-2}$, for $t_{FM} >> lm$ and $T = 300\,K$, Eq.

6.72 gives a spin-current density $J_S^z(0) \approx 10{-}8\, erg/cm^2$. Using this value for the spin-current density in Eq. 6.55; the parameters for Pt of $\lambda N = 4nm$, $\theta_{SH} = 0.08$, and $w = 0.2\, cm$; and the measured resistance $R_N = 166\Omega$, we obtain a voltage $V \approx 5\, \mu V$, which is on the order of magnitude agreement with the experimental values. And for comparison of the data of Fig.5.9 with the results of the model, it was necessary to take into account that the Pt layer resistance and the spin-Hall angle vary with T . Since there are no systematic data for the temperature dependence of the spin-Hall angle [50], we consider that the origin of R_N and the ISHE rely on the scattering of the conduction electrons in Pt and assume that $\theta_{SH}(T)$ follows the same T dependence as $R_N(T)$. The diffusion length λ_N also may vary with temperature. However, in the thickness range of our experiments, λ_N in the numerator of Eq. 6.55 approximately cancels out the one in the denominator of the tanh function.

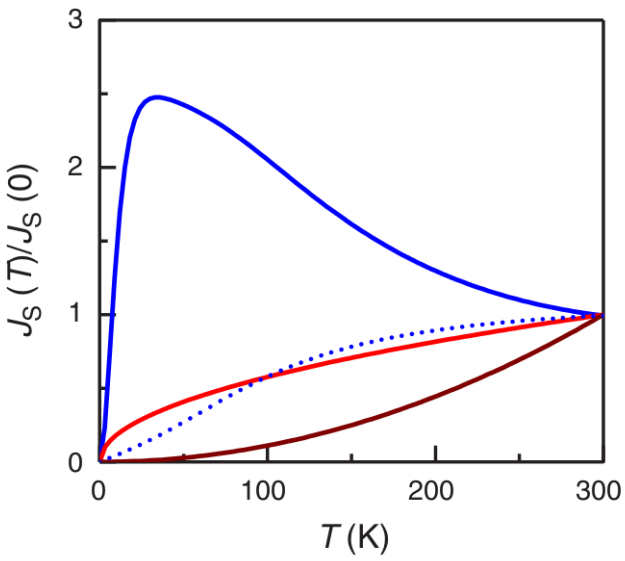

Figura 6.4: Temperature dependence of the spin current in the LSSE calculated with various models. The lower solid curve (wine) represents a T^2 dependence, as in Eq. 6.64. The solid curve in the middle (red) represents a $T^1/2$ dependence, predicted by the mechanism of interfacial thermal spin current [10]. The dotted and upper solid (blue) curves correspond to Eq. 6.72, calculated without and with, respectively, a temperature dependence in the magnon lifetime

7. CONCLUSIONS

We have presented an study of the thermal and magnetic field dependencies of the longitudinal spin Seebeck effect (LSSE) in the systems, YIG/Pt, GGG/YIG/Pt GGG/YIG/Ta and GGG/YIG/Py. The experimental results together with the theoretical model show that the mechanism behind the LSSE observed in bilayers made of a ferromagnetic insulator and a paramagnetic or ferromagnetic metal relies on the bulk magnon spin current created by the temperature gradient across the thickness of the insulator. The spin current pumped into the metallic layer provides continuity for the spin current at the interface, and it is essential for the existence of the SSE and its detection by the voltage created by the ISHE. It was observed that the LSSE do not depend of the intensity of the magnetic field when the ferromagnetic insulator is in the micrometric scale. However, when the thickness is large enough to give rise to a demagnetization energy the angular dependence of inverse spin hall effect in the metallic layer is governed by the magnetization of the FMI and there is a hysteresis-like behavior in the V_{ISHE} vs. $\vec{H}$ curve. The dependence of the LSSE with the temperature difference is linear. When the base temperature varies in a large range, the competing contributions of the magnon accumulation and relaxation rate produces a bump in the temperature dependence.

REFERENCES

[1] G.E.W. Bauer, E. Saitoh, and B.J. van Wees, Nature Mat. **11**, 391 (2012).

[2] K. Ando, S. Takahashi, J. Ieda, Y. Kajiwara, H. Nakayama, T. Yoshino, K. Harii, Y. Fujikawa, M. Matsuo, S. Maekawa and E. Saitoh, J. Appl. Phys. **109**, 103913 (2011).

[3] C. M. Jaworski, J. Yang, S. Mack, D.D. Awschalom, J.P. Heremans, and R.C. Myers, Nature Mater. **9**, 898 (2010).

[4] C.M. Jaworski, J. Yang, S. Mack, D.D. Awschalom, R.C. Myers, and J.P. Heremans, Phys. Rev. Lett. **106**, 186601 (2011).

[5] C.M. Jaworski, R.C. Myers, E. Johnston-Halperin, and J.P. Heremans, Nature **487**, 210 (2012).

[6] Rezende, S. M., Rodríguez-Suárez, R. L., Cunha, R. O., Rodrigues, A. R., Machado, F. L. A., Fonseca Guerra, G. A., Lopez Ortiz, J. C. and Azevedo, A., Phys. RevB. **89**. 014416 (2014).

[7] A.B. Harris, Phys. Rev. **132**, 2398 (1963).

[8] M. Weiler, M. Althammer, F.D. Czeschka, H. Huebl, M.S. Wagner, M. Opel, I.-M. Imort, G. Reiss, A. Thomas, R. Gross, and S.T.B. Goennenwein, Phys. Rev. Lett. **108**, 106602 (2012).

[9] A. Kehlberger, R. Röser, G. Jakob, M. Kläui, U. Ritzmann, D. Hinzke, U. Nowak, M.C. Onbasli, D.H. Kim, C.A. Ross, M.B. Jungfleisch and B. Hillebrands, arXiv:1306.0784 (2013).

[10] J. Xiao, G.E.W. Bauer, K. Uchida, E. Saitoh, and S. Maekawa, Phys. Rev. B **81**, 214418 (2010).

[11] Shun-Qing Shen, AAPPS Bulletin October, **18**, 5 (2008).

[12] Stern, O. and Gerlach, W., Zeitschrift f r Physik, **9**(1), 353-355 (1922).

[13] Johnson, Mark and Silsbee, R. H., Phys. Rev. Lett. **55** (17), 1790-1793 (1985).

[14] Aronov, A. G., JETP Lett. **24**, 32 (1976).

[15] Meservey, R., Paraskevopoulus, D. y Tedrow, P. M., Phys. Rev. Lett. **37**, 858 (1976).

[16] Grünberg, P. and Schreiber, R. and Pang, Y. and Brodsky, M. B. and Sowers, H., Phys. Rev. Lett. **57** (19), 2442-2445 (1986).

[17] Binasch, G. and Grünberg, P. and Saurenbach, F. and Zinn, W., Phys. Rev. B. **39**(7), 4828-4830 (1989).

[18] Baibich, M. N., Broto, J. M., Fert, A., Van Dau, F. Nguyen, Petroff, F., Etienne, P., Creuzet, G., Friederich, A. and Chazelas, J., Phys. Rev. Lett. **61**(21), 2472–2475 (1988).

[19] W. Thomson, Proceedings of the Royal Society of London, 8, 546-550 (1856-1857).

[20] Saburo Takahashi and Sadamichi Maekawa, Science and Technology of Advanced Materials, **9** (1), 014105 (2008).

[21] Spin Current, Edited by Sadamichi Maekawa, Sergio O. Valenzuela, Eiji Saitoh and Takashi Kimura, 400 pp. (2012).

[22] Y. Tserkovnyak, A. Brataas, G. E. Bauer, Phys. Rev. B **66**, 224403 (2002).

[23] Tserkovnyak, Yaroslav and Brataas, Arne and Bauer, Gerrit E. W., Phys. Rev. Lett. **88**. 117601 (2002).

[24] Hall, E.H., American Journal of Mathematics, **2**, 287-292 (1879).

[25] E. H. Hall, Philos. Mag. **12**, (74),157 (1881).

[26] R. Karplus and J. M. Luttinger, Phys. Rev. **95**, (5), 1154 (1954).

[27] J. Smit, Physica, **24**,(1–5),39 (1958).

[28] L. Berger, Phys. Rev. B, **2**, (11) 4559 (1970).

[29] T. Jungwirth, Q. Niu, and A. H. MacDonald, Phys. Rev. Lett. **88**, (20), 207208 (2002).

[30] S. Murakami, N. Nagaosa, and S.-C. Zhang, Science, **301**, (5638), 1348 (2003).

[31] J. Sinova, D. Culcer, Q. Niu, N. A. Sinitsyn, T. Jungwirth, and A. H. MacDonald, Phys. Rev. Lett. **92**, (12), 126603 (2004).

[32] G. Y. Guo, S. Murakami, T.-W. Chen, and N. Nagaosa, Phys. Rev. Lett. **100**, (9), 096401 (2008).

[33] T. Tanaka, H. Kontani, M. Naito, D. S. Hirashima, K. Yamada, and J. Inoue, Phys. Rev. B, **77**, (16) 165117 (2008).

[34] Y. Tian, L. Ye, and X. Jin, Phys. Rev. Lett. **103**, (8), 087206 (2009).

[35] Dyakonov, M.I. and Perel, V.I., Physics Letters A, **35** (6), 459-460 (1971).

[36] E. Saitoh, M. Ueda, H. Miyajima, and G. Tatara, Appl. Phys. Lett. **88**, 182509 (2006).

[37] N.S. Averkiev and M.I. Dyakonov, JETP Lett. **35**, 196 (1983).

[38] A. A. Bakun, B. P. Zakharchenya, A. A. Rogachev, M. N. Tkachuk, and V. G. Fleisher, Sov. Phys. JETP Lett. **40** (11), 1293 (1984).

[39] Hirsch, J. E., Phys. Rev. Lett. **83**, 1834-1837 (1999).

[40] Kato, Y. K., Myers, R. C., Gossard, A. C. and Awschalom, D. D., Science, **306**(5703), 1910-1913 (2004).

[41] A. Azevedo, L. H. Vilela Leão, R. L. Rodriguez-Suarez, A. B. Oliveira, and S. M. Rezende, J. Appl. Phys. **97**, 10C715 (2005).

[42] H. Y. Inoue, K. Harii, K. Ando, K. Sasage, and E. Saitoh, J. Appl. Phys. **102** (8), 083915 (2007).

[43] K. Ando, Y. Kajiwara, S. Takahashi, S. Maekawa, K. Takemoto, M. Takatsu, and E. Saitoh, Phys. Rev. B, **78** (1), 014413 (2008).

[44] K. Harii, K. Ando, H. Y. Inoue, K. Sasage, and E. Saitoh, J. Appl. Phys. **103** (7), 07F311 (2008).

[45] Wunderlich, J. and Kaestner, B. and Sinova, J. and Jungwirth, T., Phys. Rev. Lett. **94** (4), 047204 (2005).

[46] O. Mosendz, J.E. Pearson, F.Y. Fradin, G.E. Bauer, S.D. Bader, and A. Hoffmann, Phys. Rev. Lett. **104**, 046602 and O. Mosendz, V. Vlaminck, J.E. Pearson, F.Y. Fradin, G.E. Bauer, S.D. Bader, and A. Hoffmann, Phys. Rev. B **82**, 214403 (2010).

[47] L. Liu, C.-F. Pai, Y. Li, H. W. Tseng, D. C. Ralph, and R. A. Buhrman, Science, **336** (6081), 555 (2012).

[48] C.-F. Pai, L. Liu, H. W. Tseng, D. C. Ralph, and R. A. Buhrman, Appl. Phys. Lett. **101** (12), 122404 (2012).

[49] Y. Kajiwara, K. Harii, S. Takahashi, J. Ohe, K. Uchida, M. Mizuguchi, H. Umezawa, K. Kawai, K. Ando, K. Takanashi, S. Maekawa, and E. Saitoh, Nature (London) **464**, 262 (2010). Caloritronics References

[50] A. Hoffmann, IEEE Trans. Mag. **49**, 5172 (2013).

[51] M. Johnson, Solid State Commun. **150** 543-547 (2010).

[52] Bauer, G. E., MacDonald, A. H. & Maekawa, S. Spin caloritronics. Solid State Commun. **150**, 459-460 (2010).

[53] Ashcroft, N. W. & Mermin, N. D. Solid State Physics, Saunders (1976).

[54] M. Johnson and R.H. Silsbee, Phys. Rev. B **35**, 4959 (1987).

[55] J. Sakurai, M. Horie, S. Araki, H. Yamamoto, T. Shinjo, J. Phys. Soc. Japan **60** (1991) 2522.

[56] J. Shi, K. Pettit, E. Kita, S. S. P. Parkin, R. Nakatani, M. B. Salamon, Phys. Rev. B**54** 15273, (1996).

[57] M. Johnson, J. Supercond. **16**, pp. 679 (2003).

[58] A. Fukushima, K. Yagami, A. A. Tulapurkar, Y. Suzuki, H. Kubota, A. Yamamoto, S. Yuasa, Jpn. J. Appl. Phys. **44** L12 (2005).

[59] O. Tsyplyatyev, O. Kashuba, V. I. Fal'ko, Phys. Rev. B **74**, 132403 (2006).

[60] Gravier, L., Serrano-Guisan, S., Reuse, F. & Ansermet, J. P. Thermodynamic description of heat and spin transport in magnetic nanostructures. Phys. Rev. B **73**, 024419 (2006).

[61] M. Hatami, G. E. W. Bauer, Q. Zhang, and P. J. Kelly, Phys. Rev. Lett. **99**, 066603 (2007).

[62] M. Hatami, G.E.W. Bauer, Q. Zhang, and P.J. Kelly, Phys. Rev. B **79**, 174426 (2009).

[63] A.A. Kovalev and Y. Tserkovnyak, Phys. Rev. B **80**, 100408 (2009).

[64] R. Huber, P. Klemm, S. Neusser, B. Botters, A. Wittmann, M. Weiler, et al. , Solid State Commun. **150** 492-495 (2010).

[65] B. L. Zink, A. D. Avery, R. Sultan, D. Bassett, M. R. Pufall, Solid State Commun. **150** 514-518 (2010).

[66] T. Seki, I. Sugai, Y .Hasegawa, S. Mitani, K. Takanashi, Solid State Commun. **150** 496-499 (2010).

[67] X. Liu, X. C. Xie, Solid State Commun. **150** 471-474 (2010).

[68] Z. Ma, Solid State Commun. **150** 510-513 (2010).

[69] J. E. Wegrowe, Solid State Commun. **150** 519-523 (2010).

[70] K.M.D. Hals, A. Brataas, and G.E.W. Bauer, Solid State Commun. **150**, 461 (2010).

[71] P. Möhrke, J. Rhensius, J.-U. Thiele, L.J. Heyderman, M. Klui, Solid State Commun. **150** 489-491 (2010).

[72] Z. Yuan, S. Wang, and K. Xia, Solid State Commun. **150**, 548 (2010).

[73] T. T. Heikkila, M. Hatami, G. E. W. Bauer, Solid State Commun. **150** 475-479 (2010).

[74] M. Hatami, G.E.W. Bauer, S. Takahashi, and S. Maekawa, Solid State Commun. **150**, 480 (2010).

[75] C. -P. Chuu, M. -C. Chang, Q. Niu, Solid State Commun. **150** 533-537 (2010).

[76] V. V. Maslyuk, S. Achilles, I. Mertig, Solid State Commun. **150** 500-504 (2010).

[77] G.E.W. Bauer, A.H. MacDonald, and S. Maekawa, Solid State Commun. **150**, 459 (2010).

[78] A. A. Tulapurkar,Y. Suzuki, Solid State Commun. **150** 466-470 (2010).

[79] B. Balke, S. Ouardi, T. Graf, J. Barth, C. G. F. Blum, G. H. Fecher, et al., SolidState Commun. **150** (2010).

[80] H. Yu, S. Granville, D.P. Yu, and J.-Ph. Ansermet, Phys. Rev. Lett. **104**, 146601 (2010).

[81] W. Jiang, P. Upadhyaya, Y. Fan, J. Zhao, M. Wang, L.-Te Chang, M. Lang, K.L. Wong, M. Lewis, Y.-T. Lin, J. Tang, S. Cherepov, X. Zhou, Y. Tserkovnyak, R.N. Schwartz, and K.L. Wang, Phys. Rev. Lett. **110**, 177202 (2013).

[82] Dubi, Y. & Di Ventra, M., Phys. Rev. B **79**, 081302 (2009).

[83] K. Uchida, S. Takahashi, K. Harii, J. Ieda, W. Koshibae, K. Ando, S. Maekawa, and E. Saitoh, Nature **455**, 778 (2008).

[84] M. Morota, Y. Niimi, K. Ohnishi, D. H. Wei, T. Tanaka, H. Kontani, T. Kimura, and Y. Otani, Phys. Rev. B, vol. **83** (17) 174405 (2011).

[85] Wong, C. H., van Driel, H. J., Kittinaradorn,R.,Stoof, H. T. C. & Duine, R. A. Spin caloritronics in noncondensed Bose gases.

[86] Seebeck, Abh. K. Akad. Wiss., Berlin, 289 (1821).

[87] Seebeck, T.J., Abh. K. Akad. Wiss., Berlin, 265 (1823).

[88] T.J. Seebeck, Repts. Prussian Acad. Sci. (1823).

[89] T.J. Seebeck, Abhandlungen der Deutschen Akademie der Wissenshaften zu Berlin, 265 (1825).

[90] Barnard, R. D. Thermoelectricity in Metals and Alloys, Taylor and Francis Ltd, (1972).

[91] K. Uchida, S. Takahashi, J. Ieda, K. Harii, K. Ikeda, W. Koshibae, S. Maekawa, and E. Saitoh, Journal of Applied Physics **105**, 07C908 (2009).

[92] T. Valet and A. Fert, Phys. Rev. B. **48**, 7099 (1993).

[93] K. Uchida, H. Adachi, T. Ota, H. Nakayama, S. Maekawa, and E. Saitoh, Appl. Phys. Lett. **97**, 172505 (2010).

[94] K. Uchida, T. Nonaka, T. Ota, H. Nakayama, and E. Saitoh, Appl. Phys. Lett. **97**, 262504 (2010).

[95] K. Uchida, T. Ota, H. Adachi, J. Xiao, T. Nonaka, Y. Kajiwara, G.E.W. Bauer, S. Maekawa, and E. Saitoh, J. Appl.Phys. **111**, 103903 (2012).

[96] K. Uchida, T. Nonaka, T. Kikkawa, Y. Kajiwara, and E. Saitoh, Phys. Rev. B **87**, 104412 (2013).

[97] A. Slachter, F.L. Bakker, J.P. Adam, and B.J. van Wees, Nature Phys. **6**, 879 (2010).

[98] S. Bosu, Y. Sakuraba, K. Uchida, K. Saito, T. Ota, E. Saitoh, and and T.Takanashi, Phys. Rev. B **83**, 224401 (2011).

[99] S.Y. Huang, W.G. Wang, S.F. Lee, J. Kwo, and C.L. Chien, Phys. Rev. Lett. **107**, 216604 (2011).

[100] M.V. Costache, G. Bridoux, I. Neumann, and S. Valenzuela, Nature Mater. **11**, 199 (2011).

[101] T. Kikkawa, K. Uchida, Y. Shiomi, Z. Qiu, D. Hou, D. Tian, H. Nakayama, X.-F. Jin, and E. Saitoh, Phys. Rev. Lett. **110**, 067207 (2013).

[102] L. Lu, Y. Sun, M. Jantz, and M. Wu, Phys. Rev. Lett. **108**, 257202 (2012).

[103] M. B. Jungfleisch, A. V. Chumak, V. I. Vasyuchka, A. A. Serga, B. Obry, H. Schultheiss, P. A. Beck, A. D. Karenowska, E. Saitoh, and B. Hillebrands Appl. Phys. Lett. **99**, 182512 (2011).

[104] A. V. Chumak, A. A. Serga, M. B. Jungfleisch, R. Neb, D. A. Bozhko, V. S. Tiberkevich, and B. Hillebrands, Appl. Phys. Lett. **100**, 082405 (2012).

[105] M.B. Jungfleisch, T. An, K. Ando, Y. Kajiwara, K. Uchida, B.I Vasyuchka, A. V. Chumak, A. A. Serga, E. Saitoh, and B. Hillebrands, Appl. Phys. Lett. **102**, 062417 (2013).

[106] T. An, V.I. Vasyuchka, K. Uchida, A.V. Chumak, K. Yamaguchi, K. Harii, J. Ohe, M.B. Jungfleisch, Y. Kajiwara, H. Adachi, B. Hillebrands, S. Maekawa, and E. Saitoh, Nature Mater. **12**, 549 (2013).

[107] B. Obry, V. I. Vasyuchka, A. V. Chumak, A. A. Serga, and B. Hillebrands, Appl. Phys. Lett. **101**, 192406 (2012).

[108] R.O. Cunha, E. Padrón-Hernández, A. Azevedo, and S.M. Rezende, Phys. Rev. B **87**, 184401 (2013).

[109] G. L. da Silva, L. H Vilela-Leão, S. M. Rezende, and A. Azevedo, Appl. Phys. Lett. **102**, 012401 (2013).

[110] S. D. Brechet, F. A. Vetro, E. Papa, S. E. Barnes, and J. P. Ansermet, Phys. Rev. Lett. **111**, 087205 (2013).

[111] M. Walter, J. Walowski, V. Zbarsky, M. Munzenberg, M. Schafers, D. Ebke, G. Reiss, A. Thomas, P. Peretzki, M. Seibt, J.S. Moodera, M. Czerner, M. Bachmann, and C. Heiliger, Nat. Mater. **10**, 742 (2011).

[112] Liquid Phase Epitaxy of Electronic, Optical and Optoelectronic Materials, edited by P. Capper, M. Mauk, pp 21-43, John Wiley (2007).

[113] S. Hoffmann, K. Sato, and Y. Tserkovnyak, Phys. Rev. B **88**, 064408 (2013).

[114] B. F. Miao, S.Y. Huang, D. Qu, and C. L. Chien, Phys. Rev. Lett. **111**, 066602 (2013).

[115] A. Azevedo, O. Alves Santos, G. A. Fonseca Guerra, R. O. Cunha, R. Rodríguez-Suárez, and S. M. Rezende, Applied Physics Letters 104, 052402 (2014).

[116] S.S.-L. Zhang and S. Zhang, Phys. Rev. Lett. **109**, 096603 (2012).

[117] S.S.-L. Zhang and S. Zhang, Phys. Rev. B **86**, 214424 (2012).

[118] Y. Takezoe, K. Hosono,A. Takeuchi, and G.Tatara, Phys. Rev. B **82**, 094451 (2010).

[119] C. Heide, Phys. Rev. Lett. **87**, 197201 (2001).

[120] M. Agrawal,V. I. Vasyuchka, A. A. Serga, A. D. Karenowska, G. A. Melkov, and B. Hillebrands, Phys. Rev. Lett. **111**, 107204 (2013).

[121] Y. Tserkovnyak, A. Brataas, G. E. Bauer and B. I. Halperin, Rev. Mod. Phys. **77**, 1375 (2005).

[122] V. Castel, N. Vlietstra, and B. J. van Wees, and J. Ben Youssef, Phys. Rev. B **86**, 134419 (2012).

[123] M. Sparks, Ferromagnetic Relaxation, Mc Graw-Hill, New York (1964).

[124] S.M. Rezende, R. L. Rodríguez-Suárez, and A. Azevedo, Phy. Rev. B **88**, 014404 (2013).

[125] M.A. Gilleo and S. Geller, Phys. Rev. **110**, 73 (1958).

APPENDIX

Here, we present parameters for the calibration of the thermocouple junctions for the Cu-constantan-Cu differential thermometer. The first derivative of the calibration curve shown in Fig. 5.8 was fitted to the equation:

$$V(mV) = A + B1 * T^1 + B2 * T^2 + B3 * T^3 + B4 * T^4, \tag{.1}$$

the tables below show the parameters corresponding to each temperature range as defined by the colors of Fig. 5.8.

Range: (3.15-19.15) K

Residual Sum of Squares	5.768.002		
Adj. R-Square	0.99995		
	Parameter	Value	Standard Error
1st Deriv	A	-7,57E+14	2,79E+14
1st Deriv	B1	-4,59E+14	1,79E+14
1st Deriv	B2	-1,04E+14	4,31E+13
1st Deriv	B3	-1,04E+13	4,61E+11
1st Deriv	B4	-3,89E+11	1,85E+11

Range: (20,15-136,15) K

Residual Sum of Squares	251.856		
Adj. R-Square	0.99994		
	Parameter	Value	Standard Error
1st Deriv	A	-569.477.359	21.214.341
1st Deriv	B1	-346.841.229	1.628.468
1st Deriv	B2	-7.112.657	466.864
1st Deriv	B3	-5.185.991	592.468
1st Deriv	B4	-0.47607	0.28083

Range: (137,15-270,15) K

Residual Sum of Squares	0.02288		
Adj. R-Square	0.99999		
	Parameter	Value	Standard Error
1st Deriv	A	2.553.301	0.01011
1st Deriv	B1	-225.088	0.03002
1st Deriv	B2	-0.3139	0.02669
1st Deriv	B3	-0.15502	0.00894
1st Deriv	B4	-0.00204	1,00E+02

Range: (271,15-404,15) K

Residual Sum of Squares	0.00164		
Adj. R-Square	0.99999		
	Parameter	Value	Standard Error
1st Deriv	A	2.588.816	0.00167
1st Deriv	B1	-141.584	0.00422
1st Deriv	B2	0.08519	0.0031
1st Deriv	B3	2,71E+01	8,27E+01
1st Deriv	B4	-1,31E+01	7,21E+00

Range: (405,15 -538,15) K

Residual Sum of Squares	3,89E+01		
Adj. R-Square	0.99999		
	Parameter	Value	Standard Error
1st Deriv	A	2.464.362	0.11284
1st Deriv	B1	-0.92064	0.05121
1st Deriv	B2	0.03408	0.00854
1st Deriv	B3	-6,32E+00	6,21E+01
1st Deriv	B4	-2,26E+00	1,66E+00

Range: (539,15-673,15) K

Residual Sum of Squares	8,97E+00		
Adj. R-Square	1		
	Parameter	Value	Standard Error
1st Deriv	A	1.953.917	0.38166
1st Deriv	B1	0.06003	0.09235
1st Deriv	B2	-0.02623	0.00832
1st Deriv	B3	8,82E+01	3,30E+01
1st Deriv	B4	-6,44E-01	4,89E-01